BACHELOR'S THESIS / BIOMEDICAL ENGINEERING 2018

Unsupervised Multiple Kernel Learning to Characterize Heart Failure Patients Considering Myocardial Mechanics and Hemodynamics

Pablo Miki Martí Castellote

upf. Universitat Pompeu Fabra Barcelona

Unsupervised Multiple Kernel Learning to characterize Heart Failure patients considering myocardial mechanics and hemodynamics

Pablo Miki Martí Castellote

BACHELOR THESIS UPF / 2018

THESIS SUPERVISORS

Bart Bijnens MSc, PhD.
Sergio Sánchez-Martínez, MSc.
Scott D. Solomon, M.D.
(Brigham and Women's Hospital and Harvard Medical School, Boston, U.S.A.)

DEPARTMENT OF INFORMATION AND COMMUNICATION TECHNOLOGIES

Universitat Pompeu Fabra Barcelona

To my family, for the support here and abroad during this period of my life.

Acknowledgments

This work would not have been possible without the help and the guidance of my supervisors. For this reason I would like to thank them sincerely, as their support during the realization of this thesis has been invaluable:

- Professor Bart Bijnens for letting me perform this study within his lab and bringing me the opportunity to meet Professor Solomon.

- Sergio Sánchez-Martínez for his everyday follow-up of my work and his patience at the time of conducting this thesis. Without his personal involvement in this work my growth as a student would not have been the same.

- Professor Solomon for letting me join his research group at the Cardiology Unit at the Brigham and Women's Hospital, where aside to an incredible amount of academic baggage, I took back home the friendship of a wonderful research team.

Summary

Heart Failure with preserved Ejection Fraction has proven to be a suitable syndrome to be studied with machine learning approaches, as its complexity is not fully captured in clinical guidelines.

For this reason, in this work we present a pipeline to characterize patients from Heart Failure with Preserved Ejection Fraction cohorts. This comprises from the creation of the databases to the development of a computational platform in Python to process the images and extract the descriptors. Lastly, we implemented machine learning and dimensionality reduction techniques to explore the data and clustering and kernel regression to obtain physiological insights on the population.

We validated the Echocardiographic Image Analysis platform with clinical data from two clinical trials, succeeded at creating meaningful clusters to classify healthy and diseased patients and obtained an output space from Multiple Kernel Learning which encoded the principal modes of cardiac dysfunction.

Keywords

Heart Failure, Ejection fraction, Machine Learning, Unsupervised Multiple Kernel Learning, Kernel Regression, Clustering.

Preface

Heart Failure with Preserved Ejection Fraction (HFpEF) can be difficult to diagnose and HFpEF patients may manifest rather heterogeneous etiologies, then clinical guidelines may not fully capture its complexity.

To overcome this limitation, it seems to be helpful the analysis of various functional features of the heart. These features may ultimately be complex (e.g., patterns rather than scalar measurements), and suitable for advanced analysis through machine learning (ML). This ML analysis may help understanding the pathophysiological aspects underlying HFpEF syndrome, thus enabling identification of the different etiologies. This ultimately allows a patient-specific approach allowing for personalized-medical treatments, rather than a one-size-fits-all approach, as current clinical guidelines do. Clustering analysis of HFpEF patients by studying dense phenotypic data has been performed with promising results (SJ Shah et al. 2015). Moreover, research using unsupervised multiple kernel learning (MKL) algorithm, a non-linear dimensionality reduction technique, has already been studied using velocity traces of left ventricular walls (Sanchez-Martinez et al. 2016), with a Cohen's Kappa of 0.65 at classifying patients.

In this project we aim at providing a framework to improve the characterization of HFpEF patients by studying the patterns of the left ventricular lateral and septal wall velocities as well as the mitral and aortic blood flows, both at rest and at submaximal exercise and longitudinal strain.

INDEX

LIST OF FIGURES

LIST OF TABLES

1. INTRODUCTION: THEORETICAL FRAMEWORK

1.1 Heart Failure with preserved Ejection Fraction

The heart is the organ in charge of providing blood with enough kinetic energy to overcome the pressure gradient of the circulatory system and supply the organism with the necessary perfusion of oxygen and nutrients. For this reason, pathologies affecting its functions may result in a decrease in quality of life, comorbidities and even death [1].

Given the critical importance of the heart, evolution has ensured it has mechanisms to adapt to adverse conditions. A common ill-disposed scenario arises from a need of an increased cardiac output. To overcome this situation, heart muscle undergoes remodeling to keep up with the needs of the body. This remodeling takes place at expenses of abnormalities and eventually to the syndrome known as heart failure (HF). Among other consequences, a decrease in the pumping action may occur, valves may malfunction and the overall effect results in an enlargement, dilation and stiffening of the heart. These changes will manifest overtly unless the process can be halted [2], [3].

The previously exposed remodeling is usually due to systolic dysfunction, often caused by a myocardial infarction; diastolic dysfunction, often caused by long-term hypertension; and in multiple cases a combination of both. Other causes that lead to remodeling are the degeneration of the cardiac valves, “idiopathic” dilated cardiomyopathy and alcoholic cardiomyopathy. Less frequent causes include rheumatic valve disease and Chagas’ disease [4].

Heart failure can be divided into different classes depending on the parameter at hand. For instance, which heart side is affected (right or left), instauration time (acute or chronic) and ejection fraction (preserved or reduced). We will focus on a subset of the latter, Heart Failure with preserved Ejection Fraction (HFpEF), for this reason we explain these two types of HF in depth. Ejection fraction (EF) is computed by dividing the amount of blood that ventricles pump in each systolic cycle by the total amount of blood they are able to store. In a healthy subject or in a patient with HFpEF, the EF will range between 50 and 70%, whereas in patients with a reduced ejection fraction it will be below 50%.

The most accurate technique to acquire this marker is either echocardiogram or magnetic resonance imaging (MRI) [2].

In HF with reduced ejection fraction (HFrEF), also known as systolic HF, the heart muscle is not able to contract adequately and, therefore, cardiac output is decreased. Given that the change in EF in HfrEF is sensible and specific, its diagnosis and treatment has resulted in a consensus by the clinical community, which slightly improves in comparison to HFpEF, but it is still a challenging condition [4].

On the other hand, the pathophysiological basis of HFpEF is not well understood, thus leading to cumbersome diagnosis. Many or most of these patients probably have diastolic dysfunction, though it is not specific as it is also present in HFrEF. The results from clinical trials hitherto are negative and do not conclude an optimal treatment modality. This may be due to the usage of scalar indexes to assess cardiac function, while the use of patterns and complex descriptors can be of more relevance[2], [3], [5].

1.1.1 Cardiac Imaging and Markers

Nowadays to assess heart function it is performed cardiac imaging. Quantitative markers obtained from imaging define an objective evaluation of the patient. Devices of frequent use include echocardiography or Doppler ultrasound procedures.

The most broadly used cardiac imaging modality due to its affordability and screening power is echocardiography. It is based on the use of an ultrasound probe that can both emit and receive, allowing for a reconstruction of the heart chambers, the velocities of the cardiac walls , Tissue Doppler Imaging (TDI), as well as the velocities of the blood flow (Doppler echocardiography). It is the primary tool for screening, follow-up of patients and overall management when suspecting heart disease. Depending on specific purposes, different types of data can be obtained [6].

Echocardiograms can be obtained under several modalities, each of them offering different type of information. Going from simple to complex, B-mode (brightness mode) provides a still 2D gray-scale image of the heart. It sends a pulse from the piezoelectric crystal of the probe that automatically works as a receiver. As the time to receipt and

distance are proportional, a gray scale image can be obtained relating brightness to wave reflection change, thus soft tissue to bone would appear as white and so would soft tissue to air. Next on, M-mode (motion mode) is based on the representation of a narrow ultrasound window acquired as in B-mode but instead it is represented in time. This allows for the analysis of motion of structures such as the valve leaflets [6].

Doppler ultrasound uses the Doppler principle to obtain the velocities in a given window. It is used, depending on the gain and filtering parameters, to obtain the velocities either from blood flow or from tissues. It can be obtained in Continuous Wave (CW) or Pulsed Wave (PW). CW is obtained producing a continuous sinusoidal signal with the probe. It lacks spatial resolution but has a precise velocity resolution. Thus it is used to know the highest velocity in a given line of imaging. On the other hand, PW transmits pulses along a particular line through the tissue at a constant pulse repetition frequency (PRF). However, rather than acquiring the complete RF signal as a function of time (as in the M-mode acquisition) only one sample of each reflected pulse is taken at a fixed time, the so-called range gate, after the transmission of the pulse. Consequently, information is obtained from one specific spatial position, where velocities can be obtained [6].

Lastly, speckle tracking exploits the use of so-called fingerprints in B-mode, regions of the heart that can be traced from frame to frame. Lately, the processing of the changes in the position between each frame of these points can provide information relating to strain and motion of the cardiac tissue [6].

All in all, cardiac mechanics and hemodynamics have proven to encode information relating to the worsening of the HFpEF syndrome. Tissue Doppler imaging can yield information on how the cardiac muscle relaxes. Longitudinal strain measures relate to the distensibility of the heart, and lastly Doppler ultrasound of the blood flows can give an insight on the whole process of filling of the ventricles and ejection of blood.
The figure below -extracted from the review by R. Fontes-Carvalho and A. Leite-Moreira- illustrates how the different patterns obtained using echocardiography change depending on the severity of the condition [7], [8].

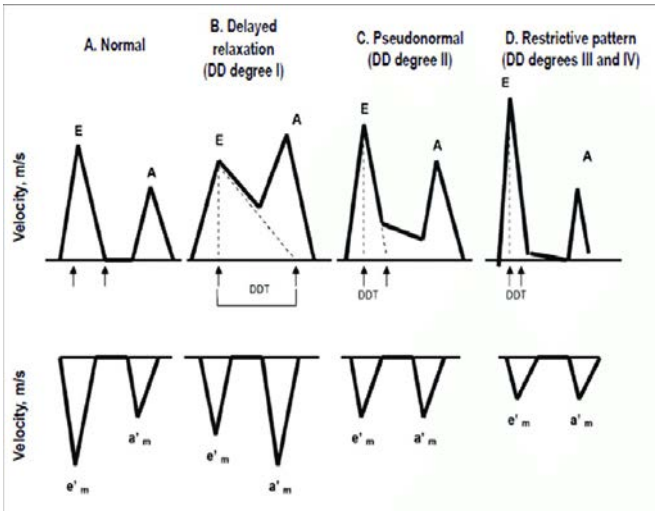

Figure 1. Mitral inflow velocity and mitral annulus velocity in different degrees of diastolic dysfunction

Echocardiography allows for the collection of several markers, we would like to emphasize two of them due to its broad use in clinical practice, especially in HFpEF: E/E'and E/A.

The E/E' ratio divides the peak of the early filling wave (E) from blood flow Doppler with the e' wave in TDI, which relates to the filling of the ventricle. This marker increases proportionally with the severity of heart failure, correlates to NT pro BNP concentration and declines as heart failure improves [9].

On the other hand, E/A ratio is computed dividing the E peak by the peak of the wave due to atrial contraction (A). It allows for a coarse profiling of the different patterns in regards to the degree of HF [2], [9].

As for biomarkers that can be measured in a blood sample, one of the most relevant is the serum concentration of natriuretic peptides. It correlates to excessive myocardial stretch, which occurs in heart remodeling. HFpEF, as well as HFrEF patients, may present slightly elevated concentrations, but these will go back to normal in asymptomatic periods. Lastly, troponin has proven to be the most accurate and specific biomarker for myocardial damage and presents strong correlation to HF [2], [9].

1.1.2 Incidence and Cost

The epidemiology of symptomatic heart failure in developed countries ranges between 1% and 2% of the adult population. Elderly people, those over the age of 65 year present an incidence of 6–10%, thus being the most prevalent group. 26 million people worldwide are living with heart failure approximately. The prognosis for HFpEF patients is poor, with survival rates worse than those for bowel, breast or prostate cancer. Healthcare expenditure is expected to increase greatly over the next decade, as patient numbers grow due to ageing populations and longer life spans.

Heart failure with preserved ejection fraction (HFpEF) accounts for almost one-half of the total heart failure burden. It presents a steady rise of its prevalence, and it appears certain that HFpEF will be the most prevalent HF type in the near future. Heart Failure supposes a cost around the 1-2% of the healthcare expenditure in developed countries. In the USA, HF is expected to cost 70 thousand million dollars in 2030 [10].

1.1.3 Clinical Guidelines

Current clinical guidelines (see Supporting Information), rely on scalar indexes and qualitative evaluation of the cardiac function. Among other markers, those used to discriminate the condition afflicting the patient are EF, E/E', E/A and BNP and NT-proBNP. Most of the cardinal symptoms (dyspnea and fatigue) and signs (peripheral edema) of heart failure are non-specific, especially in elderly patients, and could be due to other problems. Even when HF is correctly diagnosed on regards of symptoms and signs, discrimination preserved and reduced left-ventricular systolic function is difficult. Consequently, the diagnosis of heart failure requires further investigation.

Stress protocols have proven to exacerbate the symptoms as the cardiac output needs are pushed even further. We shall remind that the hearts of HFpEF patients are over the top cardiac output demands, thus exercising pushes the heart even more, not being a suitable option for improving their condition.

The most used classification of HF patients is the New York Heart Association's. It places the patients into four classes ranging from 1 being the absence of symptoms up to class 4 where there is an inability to carry any physical activity and having symptoms at rest [2].

1.2. Machine Learning

By way of introduction, in this section we will describe the basic concepts of machine learning so as to give the reader an idea of the techniques used in this project. Artificial intelligence (AI) is the field of science focused on mimicking human behavior in machines. Machine learning (ML) is a subset of AI based on statistical methods for learning a specific task. They require using the information contained in big enough datasets, from which they are able to recognize the properties and subsequently improve the task at hand. These tools are able to predict, classify or infer the true nature of data. For the sake of simplicity, we will just explain the two main modes of learning: supervised learning, if the data has been labeled with different classes, or unsupervised learning, if the algorithm is used to explore unlabeled data [11].

1.2.1. Supervised learning

In supervised approaches the learner receives a set of labeled examples as training data and makes predictions for all unseen points. This is the most common scenario associated with classification, regression, and ranking problems. One of the hottest fields at the moment is deep learning, a technique which replicates how the human brain performs computation. This means that it implements a network consisting in layers of neurons who undergo a process called back propagation to learn a task. This technique needs large amounts of data as well as big computational power, but it is able to learn how to perform very complex tasks that range from automated car driving to the prediction of cardiovascular risks from non-invasive retinal images [11].

1.2.2. Unsupervised learning

On the other hand, an unsupervised learner exclusively receives unlabeled training data, and makes predictions for all unseen points. Since in general no labeled example is available in that setting, it can be difficult to quantitatively evaluate the performance of a learner. Clustering and dimensionality reduction, on which this work focuses, are examples of unsupervised learning problems.

When dealing with high dimensional datasets, as it is the case in this project, it may be useful to create a more understandable representation. To that end, several techniques

have been created to allow for a transformation preserving the properties as much as possible between the high dimensional dataset and the low-dimensional new representation. We will illustrate an idealized example of the utility of dimensionality reduction with the figure below – extracted from the thesis of Scholz M, Approaches to analyze and interpret biological profile data.-, where small Euclidean distances in the input space become large geodesic distances in the output space [11].

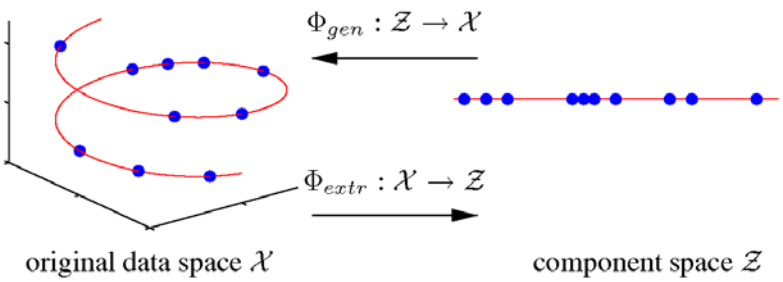

Figure 2. Dimensionality reduction

1.2.3. Potential use in HFpEF

Regarding the improvement in diagnosis of HFpEF, the biggest problem has been the etiological and pathophysiological heterogeneity of the syndrome, which favors a subset-specific rather than a uniform therapeutic approach. For this reason, in this project we exploit the evidence in the literature demonstrating that the symptomatic phase of HFpEF is characterized by abnormalities of a number of cardiac imaging markers, such as longitudinal strain as well as tissue Doppler and blood flow velocity patterns [12], [13].

Moreover, the use of statistical learning algorithms applied to more complex patterns rather than scalar indexes, may allow improved classification of heterogeneous clinical syndromes, with the ultimate goal of defining therapeutically homogeneous patient subclasses, which can potentially improve the prognosis of HFpEF [12], [13].

2. METHODS

In order to achieve the objectives set in this project, we devised a pipeline divided into two main sections. Firstly, we acquired the echocardiographic images and created a database with the images for each study. Then, a computational platform was developed to process and extract the information contained in them.

Secondly, we explored the data using an unsupervised machine learning approach. This last point consisted on three main building blocks, already explored by the work of Sánchez-Martínez et al. with satisfactory results.
The methodologies used were:

1. **Combination of features using Multiple Kernel Learning (MKL)** for fusing information from different acquisition modalities and obtaining a space of reduced dimensions [13], [14].
2. **Kernel regression along the dimensions** of the learned output space so we can observe the information encoded in them and how the features of the patients change depending on their coordinates[15].
3. Lastly, we will perform **cluster analysis** of the output space, to see if it can be a framework for the creation of HFpEF phenotype classes [12], [13].

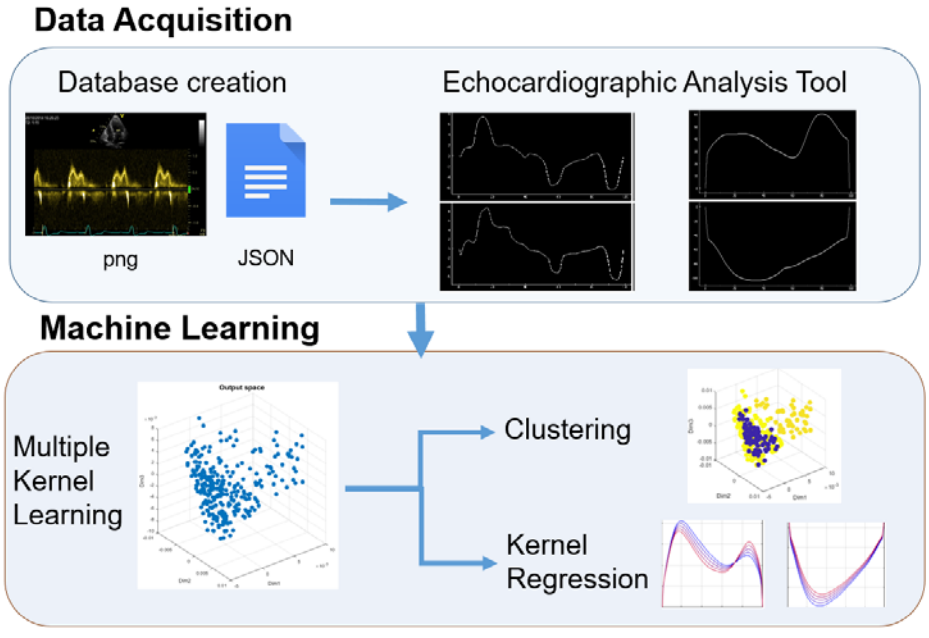

Figure 3. Representation of the whole pipeline followed by this project.

2.1 Clinical trials

2.1.1. The MEtabolic Road to DIAstolic Heart Failure (MEDIA)

The MEDIA consortium investigated how metabolic derangements contribute to Diastolic HF (DHF), how diagnostic algorithms for DHF can be improved by assessing metabolic risk and lastly how correction of metabolic risk can open new therapeutic perspectives for DHF. Their trial focused on obtaining results regarding metabolic risk-related mechanisms as therapeutic targets, the inclusion of biomarkers and arterial stiffness tests in diagnose algorithms and lastly the use of ant fibrotic therapy.

It began on 2011 and ended in 2016. It was a European common effort enrolling 21 centers across Europe, ranging from laboratories, universities and hospitals. The total cost of the trial was 15.9 million euro.

From this study we were able to obtain 420 images corresponding to 105 subjects, coming from the centers of Novara, Perugia, Cardiff and Oslo. These included TDI and valve velocity flows at rest and at submaximal exercise. From these 105, 72 were diagnosed - using the ESC 2007 consensus criteria for the diagnosis of HFpEF (Paulus et al., European Heart Journal, 2007) - as HFpEF and 33 were healthy. Our aim in this study was to observe if healthy or diseased patients could be separated in the output space of MKL.

2.1.2. Treatment of Preserved Cardiac Function Heart Failure with an Aldosterone Antagonist (TOPCAT)

The TOPCAT trial was a multicenter, international, randomized, double-blind trial, which enrolled 3445 patients with symptomatic heart failure and a left ventricular ejection fraction of 45% or more to receive either spironolactone (15 to 45 mg daily) or placebo. They were not able to observe statistically significant differences between those who received treatment and those who received placebo.

The data collected from this trial was provided by the Cardiovascular Imaging Cardiology Lab (CICL) at the Brigham and Women's Hospital in Boston, Massachusetts, USA.

From this study we obtained longitudinal strain patterns, which were already available from speckle tracking over B-mode images, aortic and mitral flow velocities for 273

patients. Our aim in this study was to observe differences within the HFpEF population, as all patients suffered from HF.

2.2. Echocardiographic Image Analysis platform

The data collected from both studies were DICOM images acquired with cardiac ultrasound. Given that both studies were conducted in different centers, the manufacturers of the imaging tools were also different. This had to be taken into account at the time of making the platform flexible so these different images could be read properly. The echocardiograms used were either flow velocity profiles or tissue Doppler imaging patterns. An example of each is shown in the figure below.

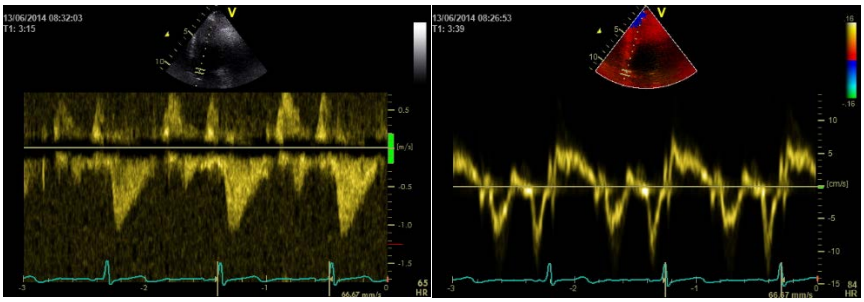

Figure 4. Doppler echocardiograms. Aortic outflow velocity (right) and septal wall velocity (left)

In the MEDIA study, subjects were studied at both rest and submaximal exercise. As previously mentioned, HF symptoms get exacerbated when increasing even further the cardiac output needs.

The patterns contained in these images are the features we want to input to the MKL algorithm. To that end, we coded a computational platform written in Python, so we can extract the information from these images. Ultimately, the platmorm outputs the patterns corresponding to both TDI and flow Doppler correctly aligned in a cardiac cycle so they can be comparable at the time of using machine learning.

The whole user interface and underlying image processing algorithms are explained down below.

Python is an open source programming language. One of its main strengths is the amount of libraries available for multiple tasks such as machine learning, image processing and creation and edition of data structures. For this and other reasons we decided to implement

the platform in this language. The whole user interface was developed using PyQt, a set of bindings which allow for the use of Qt in Python.

The algorithms and functions used were mainly from the libraries:

1. Sci-kit and OpenCV: For a broad range of image processing steps (contrast stretching, median filtering and connectivity based component removal of noise)
2. NumPy: For Signal processing and overall mathematical operations.
3. PyQtgraph: To display images, signals and the combination of both.
4. Simplejson: To read the JSON files as well as to create the files containing the paths to the images in the database.

This platform uses pairs of png images and JSON files. These are obtained by processing DICOM images through the online tool developed at UPF (https://rkt-viewer.surge.sh/), shown in the figure below. The png file contains the pixel RGB values whereas the JSON file contains the metadata of the DICOM, this information encapsulates among other things the coordinates of the image in order to crop it or the equivalency constant between a pixel and cm/s.

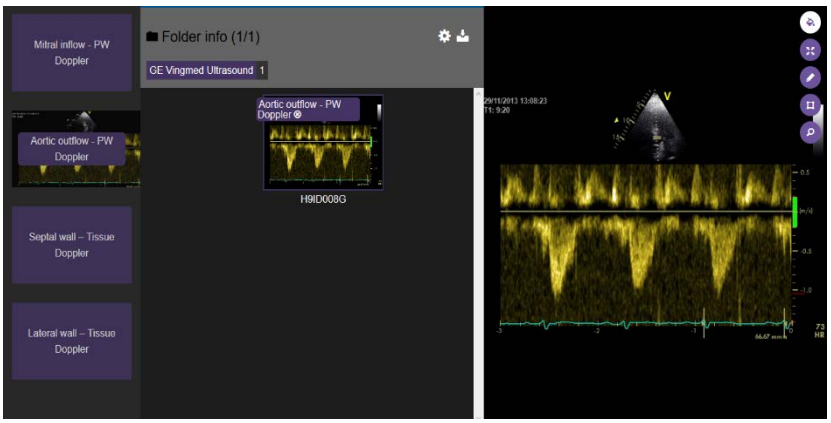

Figure 5. Image Classification Tool developed at UPF

The user interface was divided in three different compartments. From left to right, the database tree, the tissue Doppler windows and the flow velocity patterns. On top we find the septal wall velocities and the mitral inflow. At the bottom are the lateral wall image and the aortic outflow image.

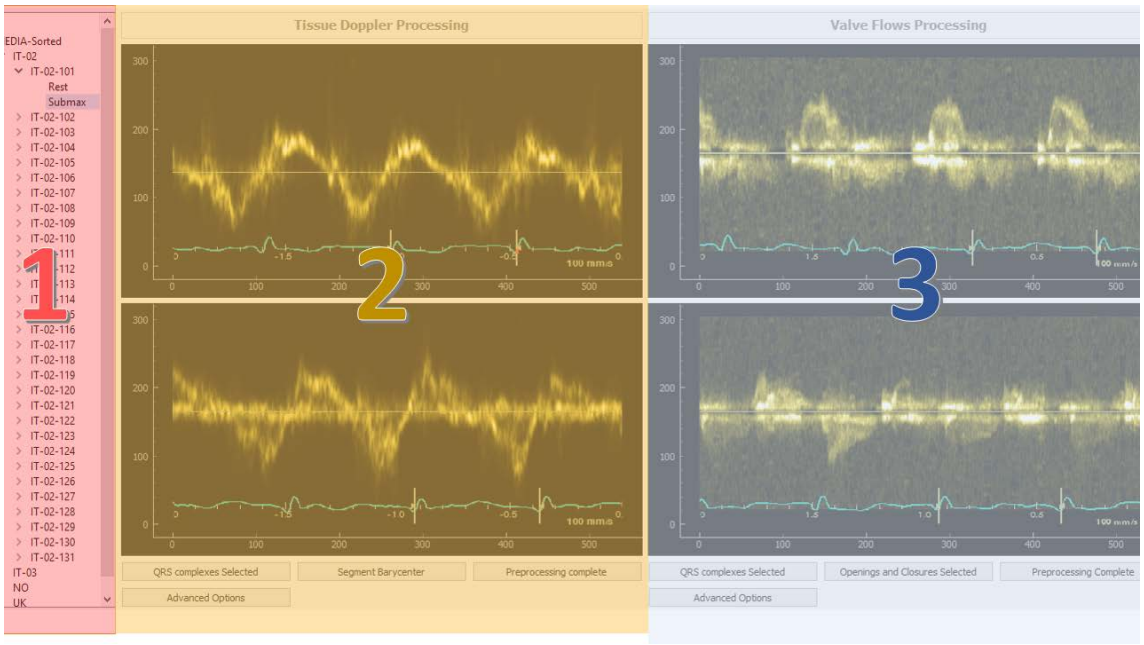

Figure 6. Representation of the Echocardiography Image Analysis tool

2.2.1. Database and image reading

Firstly, the platform reads the whole database and creates a tree structure where, hierarchically, the labels corresponding to study, center, patient ID and modality. This last makes reference to the MEDIA subjects, who underwent imaging at both rest and submaximal exercise. When clicking the specific bottom level label the platform opens the corresponding images in the windows. Then it is time to process the images.

2.2.2. Tissue Doppler Images

Tissue Doppler images provide information on the velocity of the ventricular walls. This is done by placing the reading window on top of the wall at the time of acquiring the image. Due to the very nature of the ultrasound modality, the profile produced is a yellow band around the values it takes. These images tend to contain more noise around the zero line, so the signal may get decreased at the time of extraction and high or low peaks will not be easy to capture.

The approach followed to recover the signal was to segment the barycenter of each column and adjusting for the distance to the zero line, so further values get increased in order to compensate the noise. This compensation takes place within a “weighting

window", which is comprised between two lines parallel to the zero line, at the same distance from it, one above it and the other below.

The user selects the ECG onsets, represented in red in the image, which will be used to define different cycles. Next, low pass filtering is applied to the signal with a cutoff frequency proportional to the heart rate. This means that the higher the heart rate the higher the cutoff frequency. Lastly, if there is more than one cycle, they will be averaged producing a unique, more robust descriptor.

Some parameters as the length of the weighting window and the cutoff frequency are able to be changed manually if necessary. This allows for better segmentations in some cases where the automatic algorithm has not been able to find the best values for these parameters. As a last resource strategy, manual segmentation of the signal has been implemented with the ability to place fiducial points over the image to create a signal when connecting the dots with a third degree spline.

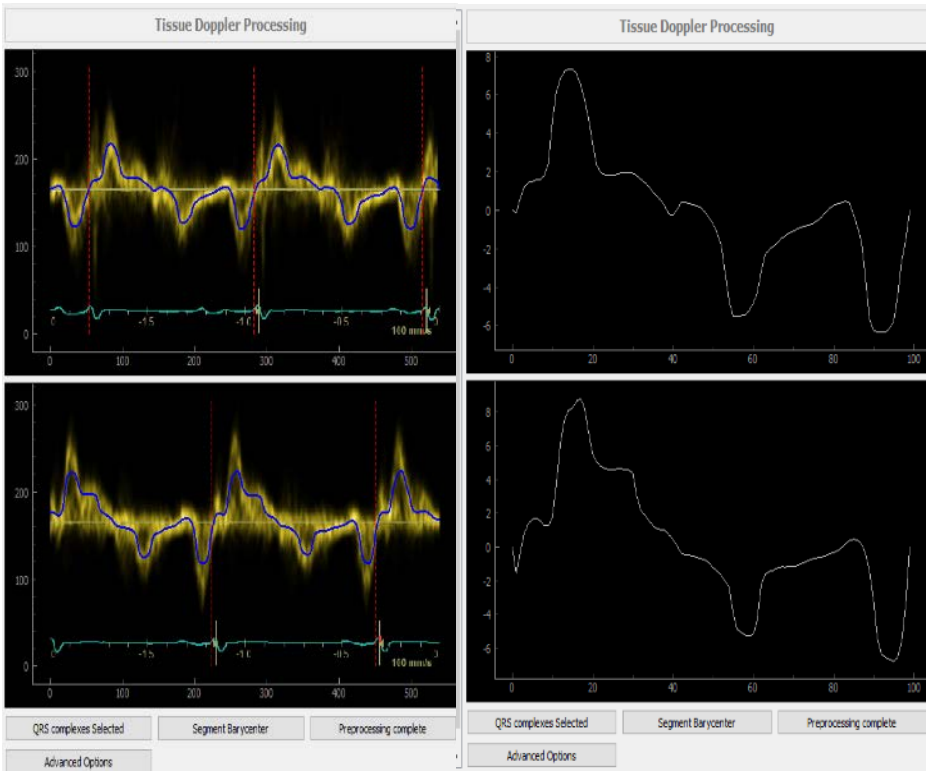

Figure 7. TDI processing

In the figure above, the left image shows the pattern computed after processing the image, this is useful if the user is not satisfied with the results and wants to refine the segmentation. On the left image, the final averaged profile is shown, the platform stores

this signal as a 1D vector containing 100 samples. This vector will be saved as a txt file within the same folder as the images.

2.2.3. Valve flow velocities

The mode of acquisition of flow velocities was pulsed-wave Doppler ultrasound. This modality is better at detecting the velocities within the window of analysis than continuous-wave Doppler where high velocities are better captured at expenses of not knowing exactly where they are produced.

Pulsed wave Doppler results in a filled pattern, so the approach followed aimed at capturing the border line of it. The extraction of these profiles contained several image processing algorithms applied sequentially in order to recover the final profile. Firstly, the user selects the valve openings and closures, as only the pattern contained within will be taken into account.

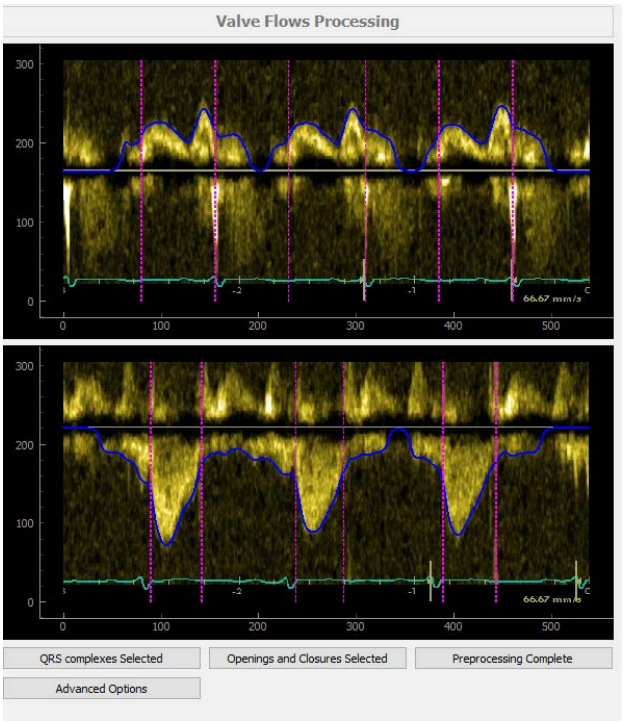

Figure 8. Flow velocity processing

Once the events have been selected, the platform starts by using contrast stretching followed by a median filter to both enhance the brightness and remove the noise known as “salt and pepper”. This leads to the next step, binarization, noise removal and hole

filling. The platform computes the optimum binarization threshold at the time of classifying the foreground, then removes spurious noise islands using connectivity based algorithms, resulting in the elimination of those “blobs” of white pixels which do not correspond to the foreground. Lastly, it fills the holes within the computed binarization to obtain a uniform segmentation.

Figure 9. Binarized flow velocity images

Once the segmentation has been obtained, another connectivity based algorithm is run column-wise to detect to detect the largest amount of non-zero pixels which correspond to the envelope of the segmentation -either on top in mitral flows or at the bottom in aortic images-. When the whole envelope is computed, the resulting profile is filtered with a low-pass filter, yielding a smoother signal.

Now that we have segmented the edges of the profile, we can extract from the JSON file the conversion constant to compute the final signal. And on the same note, if there is more than one cycle they will be averaged. The computed averaged descriptor also contains 100 samples and is stored in a txt file in the same folder as the images.

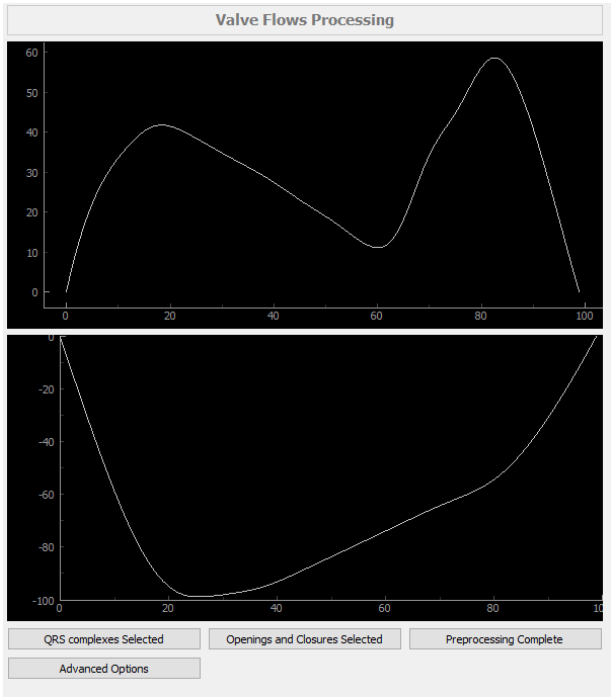

Figure 10. Blood flow velocity profiles

The user interface allows to manually change the values of the parameters corresponding to the binarization threshold and the cutoff filtering frequency, if necessary. As in TDI processing, there is also the chance to manually segment the signal placing fiducials over the flow which will then be connected through a third degree spline.

2.3. Multiple Kernel Learning (MKL)

2.3.1. General overview and rationale

Unsupervised MKL is based on the combination, linear or not, of several kernels for creating an output space that preserves similarities in the input features. A kernel is defined as a matrix of pairwise similarity between samples [14], [16].

Flow velocity patterns, longitudinal strain or tissue Doppler imaging profiles can be regarded as features of each patient -i.e. each patient could be described depending on the shape and amplitude of them- from which we can then compute a kernel, keep in mind that the patterns have been aligned to a single cardiac cycle in order to be comparable. This will result in a number of kernels equal to the number of features. These profiles will be extracted form echocardiography images using the Echocardiographic Image Analysis

platform we developed and imported into MATLAB, where the MKL algorithm was implemented.

In this project we use the unsupervised formulation of MKL to explore the data in an agnostic setting. As given the specific scenario of HFpEF, where diagnostic labels may be affected by human error due to its difficult identification, our results will not be affected by it but rather provide information about the true nature of the patients [16].

2.3.2. Mathematical insight

Following the formulation of unsupervised MKL proposed by Lin et al. and used in the work of Sánchez-Martínez et al., we define it exactly as it is shown in the literature, so consider this section being a quotation from those works.

The input data $\{ x_{m,i} \}_{(m,i) \in [1,M] \times [1,N]} \in X_m$, consist of N samples with M features each. For each feature an affinity matrix K_m is computed, using a Gaussian kernel function:

$$\mathbf{K}_m(\mathbf{x}_{m,i}, \mathbf{x}_{m,j}) = \exp\left(-\frac{\|\mathbf{x}_{m,i} - \mathbf{x}_{m,j}\|^2}{2\sigma_m{}^2}\right),$$

Where m represents the feature and i and j relate to the subjects. Once the kernel for each feature has been computed, the global affinity matrix W is computed as:

$$\mathbf{W} = \sum_{m=1}^{M} \widehat{\mathbf{K}}_m,$$

M stands for the total amount of features. $\hat{\mathbf{K}}_m = (\mathbf{K}_m)^{1/\alpha m}$ and αm results from dividing the variance of kernel $\mathbf{K}_m$ by the variance of the smallest variance kernel among the total M kernels. This prevents the highest variability features from dominating the rest of the features in the construction of the global affinity matrix $\mathbf{W}$. Then, this matrix is made sparse by retaining the entries within a fixed neighborhood ($\hat{\mathbf{W}}$). Next, we proceed to define the MKL conditions and minimization functions in a scenario with multiple features to obtain the output space with reduced dimensions.

$$\min_{\substack{\boldsymbol{\beta}\in\mathbb{R}^{M\times 1}\\ \mathbf{A}\in\mathbb{R}^{N\times N-1}}} \quad \sum_{i,j=1}^{N} \|\mathbf{A}^\top \mathbb{K}^{(i)}\boldsymbol{\beta} - \mathbf{A}^\top \mathbb{K}^{(j)}\boldsymbol{\beta}\|^2 \widehat{\mathbf{W}}_{i,j}$$

$$\text{s.t.} \quad \sum_{i=1}^{N} \|\mathbf{A}^\top \mathbb{K}^{(i)}\boldsymbol{\beta}\|^2 \mathbf{D}_{i,i} = 1,$$

$$\beta_m \geq 0, \sum_{m=1}^{M} \beta_m = 1,$$

Where D is a diagonal weight matrix, whose entries are the result of a row-wise summation of $\hat{\mathbf{W}}$. N is the number of samples, x i is the value of the only descriptor associated to sam- ple i in the input space and v is the matrix that projects it to the output space. The unknowns to the problem at hand are: **A,** the rotation matrix that maps the input to the output space, which is $N-1$ dimensional since the smallest eigenvalue is 0; and $\beta = [\beta 1 \ldots \beta_M]$, the weights given to the different features. Matrix $K^{(i)}$ is defined for the *i*-th sample as:

$$\mathbb{K}^{(i)} = \begin{bmatrix} \mathbf{K}_1(1,i) & \ldots & \mathbf{K}_M(1,i) \\ \vdots & \ddots & \vdots \\ \mathbf{K}_1(N,i) & \ldots & \mathbf{K}_M(N,i) \end{bmatrix} \in \mathbb{R}^{N\times M}.$$

Lastly, the inputs can finally be mapped to the output space using the formula:

$$\mathbf{Y} = \mathbf{A}^\top \sum_{m=1}^{M} \mathbf{K}_m \beta_m,$$

The resulting matrix $\mathbf{Y} \in R^{N-1 \times N}$ contains on each column the coordinates for each input sample $\mathbf{x}_i$ in the output space. Notice that the dimensions of the space are reduces due to the term N-1. Depending on the purpose of the experiment, the matrix **Y** can be cut down to a $d \times N$ version, this will further reduce the dimensions of the space when considering the *d* smallest eigenvalues [14], [16].

2.4. Kernel Regression

Once the output space with reduced dimensions has been obtained, we will proceed to observe how the features change when advancing in a specific dimension. Given that in our case the features are patterns of either strain, flow velocities or wall velocities, we will be able to observe how their properties change. To do so we used the technique described in the work of Bermanis et al. where a multiscale extension method is defined

for allowing the reconstruction of the features from a space obtained by using dimensionality reduction [15].
This technique may provide clinical insights, as studying which are the main modes of variation of the patterns and seeing how they might be coupled can be new physiological knowledge in the HFpEF community.

2.5. Clustering analysis

Clustering is a technique used to create groups within the data, so as to generate classes of objects that share common characteristics. To summarize, we could say that the goal is for objects within a group to be similar (or related) with one another and different from (or unrelated to) the objects in other groups. The greater the similarity (or homogeneity) within a group and the greater the difference between groups, the better or more distinct the clustering will be [11]–[13].

As proposed by the work of Shah et al., HFpEF may present different phenotypic groups, all of them suffering from the syndrome but with different underlying pathologies. In addition, different phenotypic groups may benefit from different treatment approaches, helping both diagnosis and prognosis of these patients [12].

To that end, we performed clustering so we could observe if healthy and HFpEF subjects were different in the MEDIA cohort. The algorithm used was hierarchical clustering.

The MEDIA hierarchical clustering was performed in a semi-supervised approach. We launched the clustering in a step-wise fashion. This procedure is done by feeding the algorithm n+1 dimensions in each step, starting with n=1, and computing how well these two centroids are at the time of agreeing with clinical labels [16].

To illustrate the concept of clustering, we plotted the result of applying K-means with the elbow method to the output space obtained using flow velocities and longitudinal strains in the TOPCAT cohort, but note that those clusters have not been analyzed yet.

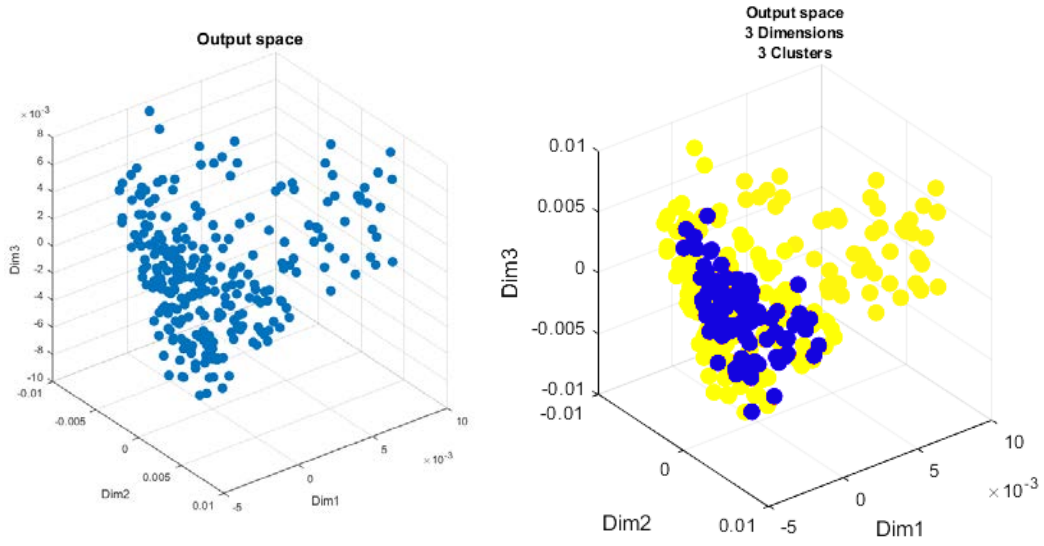

Figure 11. Clustering

Represented in different colors, we can observe the different clusters. We must note that depending on the number of dimensions we fed the clustering algorithm may produce different clusters.

3. RESULTS

3.1 Echocardiographic Image Analysis platform

To begin with, we would like to show the results obtained with the platform we developed. We validated the results by observing the profiles obtained and comparing them to the raw image from where they were extracted. Using our platform we processed 378 patients, corresponding to 966 images. The platform proved to be able at the time of reading images from the manufacturers General Electrics, Philips, ACUSON, Toshiba, Esaote, Agilent Technologies and ATL.

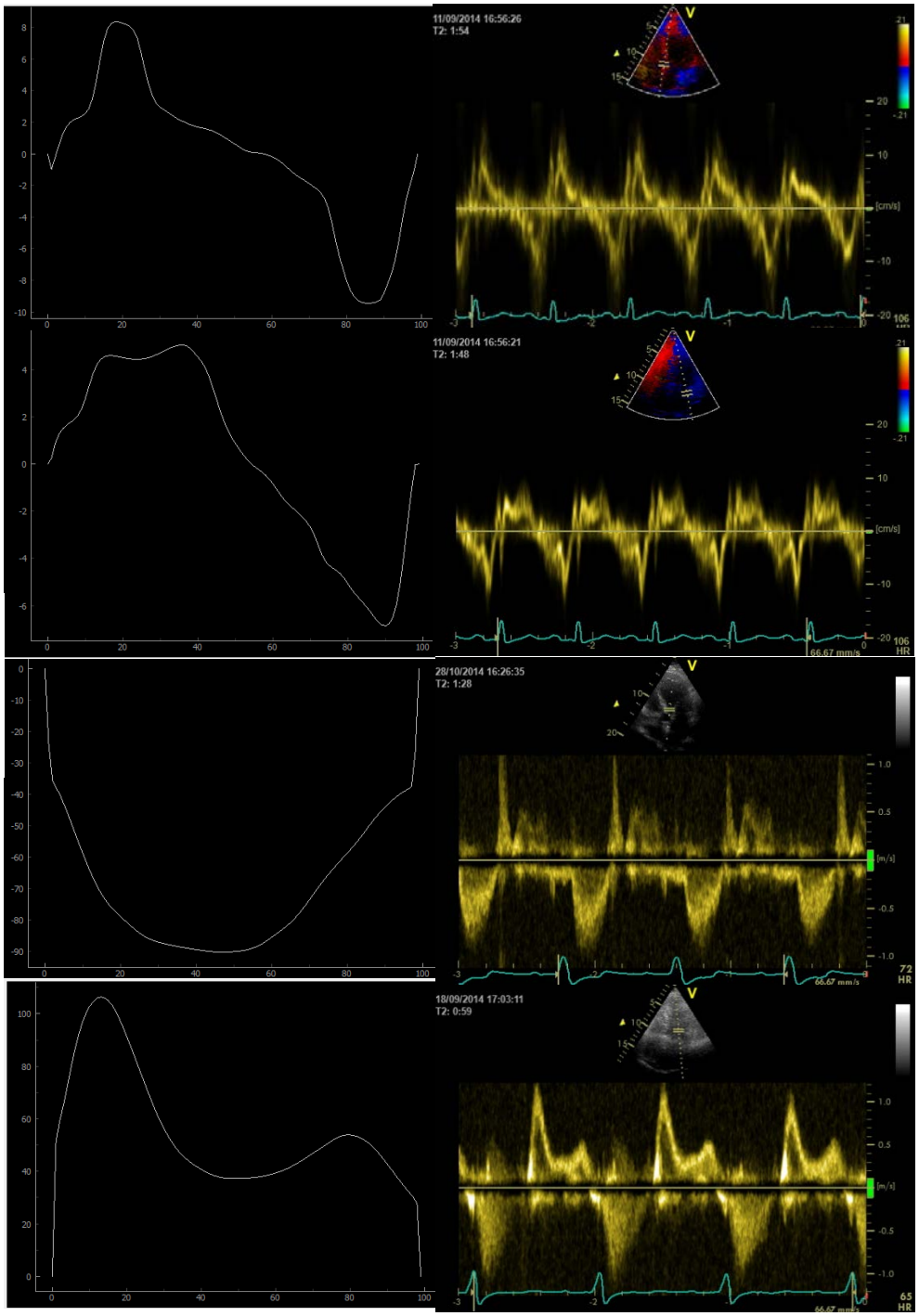

Figure 12. Validation of the Echocardiography Analysis Platform

As we can see, the profiles obtained are correct and can be used for our purpose. Both shape and amplitude are correctly preserved in the extraction of the profiles. An approximate 30% had to be segmented manually –the tuning of parameters was not enough to improve the segmentation- using the placement of fiducial points, this is due to the presence of noise in stress protocol imaging in MEDIA and also due to the difficulty of acquiring clean images in overweight patients.

In addition, and for the sake of data exploration, we plotted the profiles altogether to check that all of them fell in the correct range and there were no distant outliers. As expected, all the profiles are correct.

3.2. MEDIA

Aiming at separating both groups, diseased and healthy, we launched the MKL algorithm fusing the patterns obtained from TDI and flow velocity profiles. Once the output space was obtained, we represented the first three dimensions of the total of 104 that the MKL algorithm produces. We then represented the 33 subjects in blue and the 72 diseased in red, using the labels provided by clinical diagnosis. As it can be observed in the figure below, there is already a possible separation between them in the output space.

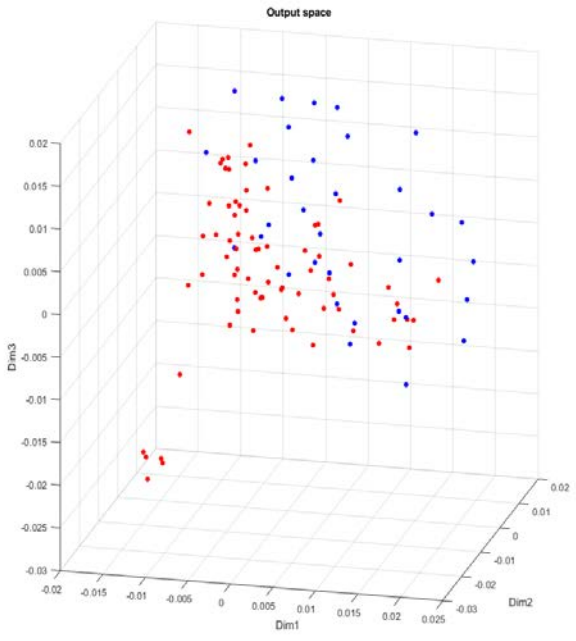

Figure 13. MKL Output space for the MEDIA cohort.

To evaluate how good this separation was, we performed the clustering as explained in section 2.3. We present the results of the algorithm in the table below, where we also tuned the kernel band-widths (first two columns) to ensure the best result. The different results are shown below, were the best agreement was found using the first nine dimensions.

KERNEL 1	KERNEL 2	SENSITIVITY	SPECIFICITY	ACCURACY	NUM. DIMS	KAPPA
16	**7**	0.90278	0.78788	0.86667	9	0.69
16	**8**	0. 91667	0. 69697	0.8472	14	0.63446
15	**7**	0.91667	0.75758	0.86667	10	0.68549
15	**8**	0.90278	0.69697	0.8381	13	0.61489
15	**9**	0.88889	0.66667	0.81905	12	0.56958
14	**7**	0.88889	0.75758	0.84762	9	0.64646
14	**8**	0.90278	0.66667	0.82857	15	0.58877
10	**10**	0.91667	0.57576	0.80952	13	0.52703

Table 1. Results of clustering

Once the two centroids were obtained, we measured the Mahalanobis distance from each subject to both centroids. It is defined as:

$$d(\mathbf{y}_i, S_c) = \sqrt{(\mathbf{y}_i - \mu_c)\boldsymbol{\Sigma}_c^{-1}(\mathbf{y}_i - \mu_c)^\top} \quad \forall\, i \in [1, N],$$

Where S_c are the class-related subgroups and $c \in$ {'healthy', 'diseased'}. Here, $\mu_c \in \mathrm{R}^d$ and $\Sigma_c \in \mathrm{R}^{d \times d}$ are the mean vector and covariance matrix of S_c. This resulted in the figure shown below.

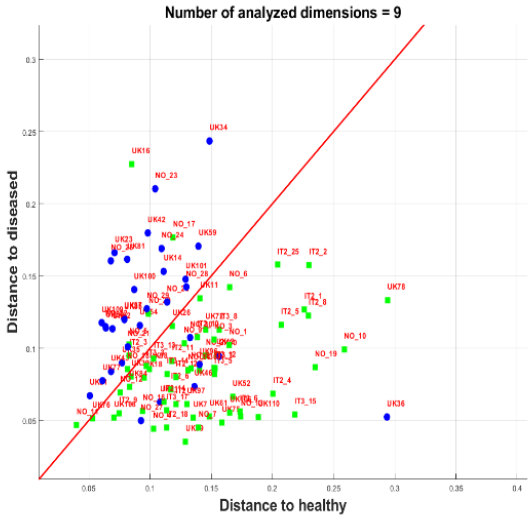

Figure 14. Mahalanobis distances to the centroids

In green we can observe the healthy controls while in blue we represented the diseased patients. The x axis encodes the distance to the healthy centroid while the y axis does it for the diseased cluster, the red line would represent an equal distance to both clusters. We shall remark that the clinical labels could contain human errors, and could be considered an approximation of ground truth.

Despite of very few outliers, most healthy subjects are closer to the healthy centroid and most diseased participants are closer to the diseased centroid. To have a quantitative assessment, we computed the sensitivity, specificity and Cohen's Kappa for this classification. The results compared to those obtained by the previous work of Sánchez-Martínez et al. are [16]:

	Present work (n=105)	**Sánchez-Martínez et al. (n=55)**
Sensitivity (%)	90.3	78.9
Specificity (%)	78.78	86.4
Cohen's Kappa (%)	69	65.5

Table 2. Comparison of results

Considering the Cohen's Kappa as the overall measure of performance, as it considers randomly classifying correctly an instance, we can say we improved the classification in an even larger cohort. Note also that the comparison cannot be straight forward as the sample size in this work is almost twice as big.

3.3. TOPCAT

As for the results obtained in the TOPCAT cohort, the kernel regression along the first four dimensions of the output space provided very interesting results.

Below we can see a series of plots, each column from left to right corresponds to the first, second, third and fourth dimensions. The five profiles shown in each plot correspond to the mean, one and two standard deviations. These patterns are synthetic, meaning that there is not necessarily any patient that has such a profile. The top row shows the mitral inflows and the bottom plots the aortic patterns.

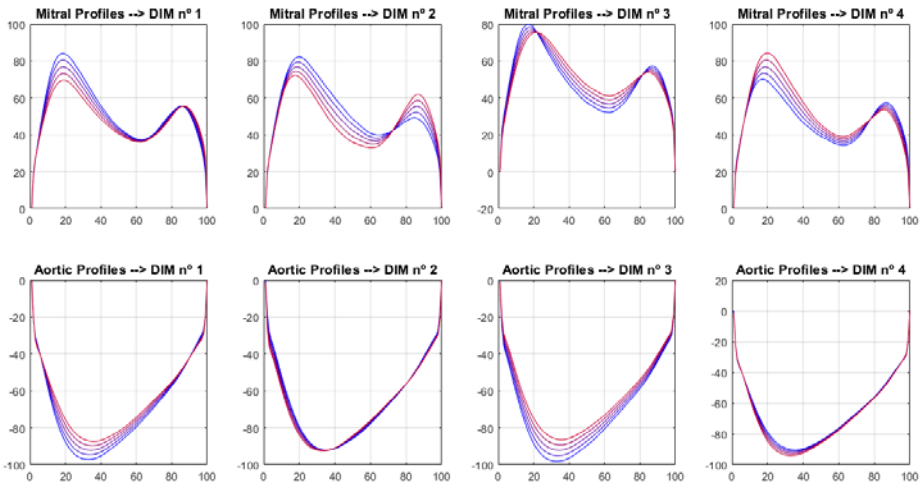

Figure 15. Kernel Regression in the first four dimensions of the output space of TOPCAT

Regarding the four first dimensions of the MKL output space we observe that:

- In **dimension one**, we observe the variability in the amplitude of the early filling peak (E) coupled with the rounding of the aortic profile.
- In **dimension two** we observe an inverse relation between the amplitude of the early filling peak (E) with the atrial contraction wave peak (A). No differences are observed regarding the aortic patterns in dimension two.
- In **dimension three**, the velocity at which the filling peaks take place is encoded. In addition, we can also observe time variability in the E peak. Moreover, coupling with the rounding of the aortic outflow is also observed in this dimension.
- **Dimension four** encodes the decrease of E while the A peak increases. Unlike dimension one, there is no coupling with the aortic profiles as they remain the same.

4. DISCUSSION AND CONCLUSION

Observing the work as a whole, we achieved three important milestones:

1. We successfully implemented and validated an **Echocardiographic Image Analysis platform** able to read databases and extract the information contained in either echocardiographic images acquired with Tissue Doppler imaging or Doppler Ultrasound from a broad range of manufacturers.
2. We were able to obtain a **separation between healthy subjects and diseased** in cohort comprised of 105 patients better than in current bibliography.
3. We were able to capture the **modes of cardiac dysfunction** in the output space of MKL learned with the TOPCAT patients.

In conclusion, being able to separate with a relatively high confidence the participants who had HFpEF from those who are healthy, strengthens the rationale of using unsupervised MKL for unraveling the complexities in this syndrome. It gives an insight on the capacity of this algorithm to agnostically learn a space in which patients can get classified. The improvement can be due to both using a larger cohort and the fusion of flow and wall velocities, which feds the algorithm with more information about how the function of the heart. Although the separation proved to be good, this findings must be validated with externally and clinical outcomes should correlate strongly with the classification

Moreover, observing the changes in both mitral and aortic flows in the same way as in the worsening described in clinical literature –see figure describing the changes in the mitral and TDI profiles - can be used to confirm the relevance of this patterns. An interesting observation we can make is the coupling between changes in both types of flows, mitral and aortic, when the disease worsens.

All in all, important results have been obtained from which even more information can be extracted. For this reason we also present a list of possible continuations to this project in the following section.

4.1. Future work

Taking into account that the building blocks of this work can be combined in a very broad number of ways, most of them able to provide new and interesting ways of exploring the data, there are many possible future experiments that can be carried out.

To begin with, regression in the clusters obtained in the MEDIA output space could shed light on the differences between healthy and disease participants, allowing for a physiological and clinical understanding of their meaningfulness. Also, regression in the dimensions of this output space could be done so as to determine which changes in the patterns correlate to being classified as healthy or diseased.

On the other hand, clustering in the TOPCAT output space should be carried out and analyzed to see which physiological differences separate the groups. If the results were significant, clinical knowledge could be produced, and phenogroups could benefit from personalized therapies.

Analyzing the solutions obtained using different features, for instance, using only the flow velocities or the tissue Doppler, would be relevant at the time of determining the role these features play at the time of creating the output space.

Finally, the isovolumic contraction time and relaxation times could be computed from the images in order to produce two more relevant features which have potential to improve the pathophysiological insights.

5. BIBLIOGRAPHY

[1] J. G. Betts *et al.*, *Anatomy and Physiology*. 2016.

[2] P. Ponikowski *et al.*, "2016 ESC Guidelines for the diagnosis and treatment of acute and chronic heart failure," *European Heart Journal*. 2016.

[3] A. Desai, "Current understanding of heart failure with preserved ejection fraction," *Current Opinion in Cardiology*. 2007.

[4] J. J. V McMurray and M. A. Pfeffer, "Heart failure," *Lancet*, 2005.

[5] A. Vazir and S. D. Solomon, "Management Strategies for Heart Failure with Preserved Ejection Fraction," *Heart Failure Clinics*. 2014.

[6] S. D. Solomon, *Atlas of Echocardiography*, Current Me. Springer US, 2009.

[7] D. K. Gupta and S. D. Solomon, "Imaging in Heart Failure with Preserved Ejection Fraction," *Heart Failure Clinics*. 2014.

[8] R. Fontes-carvalho and A. Leite-moreira, "Heart Failure with Preserved Ejection Fraction : Fighting Misconceptions for a New Approach," *Arq Bras Cardiol*, vol. 96, no. 6, pp. 504–513, 2011.

[9] W. C. Meijers, A. R. van der Velde, and R. A. de Boer, "Biomarkers in heart failure with preserved ejection fraction," *Netherlands Hear. J.*, vol. 24, no. 4, pp. 252–258, 2016.

[10] G. Savarese and L. H. Lund, "Global Public Health Burden of Heart Failure," *Card. Fail. Rev.*, 2017.

[11] E. Alpaydın, "Introduction to machine learning," *MIT Press*, 2012.

[12] S. J. Shah *et al.*, "Phenomapping for novel classification of heart failure with preserved ejection fraction," *Circulation*, vol. 131, no. 3, pp. 269–279, 2015.

[13] S. Sanchez-Martinez *et al.*, "Machine Learning Analysis of Left Ventricular Function to Characterize Heart Failure With Preserved Ejection Fraction.," *Circ. Cardiovasc. Imaging*, vol. 11, no. 4, p. e007138, 2018.

[14] Y. Lin, T. Liu, and C. Fuh, "for Dimensionality Reduction," *Tpami*, vol. 33, no. X, pp. 1–14, 2011.

[15] A. Bermanis, A. Averbuch, and R. R. Coifman, "Multiscale data sampling and function extension," *Appl. Comput. Harmon. Anal.*, 2013.

[16] S. Sanchez-Martinez, N. Duchateau, T. Erdei, A. G. Fraser, B. H. Bijnens, and G. Piella, "Characterization of myocardial motion patterns by unsupervised multiple kernel learning," *Med. Image Anal.*, vol. 35, pp. 70–82, 2017.

- SUPPORTING INFORMATION -

ESC Clinical guidelines for HFpEF

The material included in this section is directly extracted from the corresponding guidelines and has the purpose to illustrate the point presented in this project: Poor diagnosis of HFpEF patients is due to an oversimplification of the syndrome and the lack of usage of complex descriptors at the time of diagnosing.

1- European Society of Cardiology (ESC) 2016:

(https://academic.oup.com/eurheartj/article/37/27/2129/1748921#109986804)

"Symptoms are often non-specific and do not, therefore, help discriminate between HF and other problems. Symptoms and signs of HF due to fluid retention may resolve quickly with diuretic therapy. Signs, such as elevated jugular venous pressure and displacement of the apical impulse, may be more specific, but are harder to detect and have poor reproducibility.

Symptoms and signs may be particularly difficult to identify and interpret in obese individuals, in the elderly and in patients with chronic lung disease. Younger patients with HF often have a different etiology, clinical presentation and outcome compared with older patients".

Symptoms	Signs
Typical	**More specific**
Breathlessness Orthopnoea Paroxysmal nocturnal dyspnoea Reduced exercise tolerance Fatigue, tiredness, increased time to recover after exercise Ankle swelling	Elevated jugular venous pressure Hepatojugular reflux Third heart sound (gallop rhythm) Laterally displaced apical impulse
Less typical	**Less specific**
Nocturnal cough Wheezing Bloated feeling Loss of appetite Confusion (especially in the elderly) Depression Palpitations Dizziness Syncope Bendopnea[63]	Weight gain (>2 kg/week) Weight loss (in advanced HF) Tissue wasting (cachexia) Cardiac murmur Peripheral oedema (ankle, sacral, scrotal) Pulmonary crepitations Reduced air entry and dullness to percussion at lung bases (pleural effusion) Tachycardia Irregular pulse Tachypnoea Cheyne Stokes respiration Hepatomegaly Ascites Cold extremities Oliguria Narrow pulse pressure

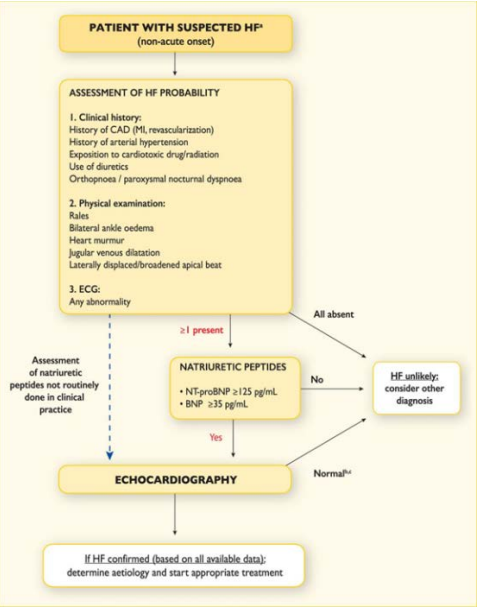

Relating to the scalar indexes discussed in this dissertation it says:

"A normal ECG and/or plasma concentrations of BNP <35 pg/mL and/or NT-proBNP <125 pg/mL make a diagnosis of HFpEF, HFmrEF or HFrEF unlikely.

- The presence of symptoms and/or signs of HF (see *Table 4.1*)
- A 'preserved' EF (defined as LVEF ≥50% or 40–49% for HFmrEF)
- Elevated levels of NPs (BNP >35 pg/mL and/or NT-proBNP >125 pg/mL)
- Objective evidence of other cardiac functional and structural alterations underlying HF (for details, see below)
- In case of uncertainty, a stress test or invasively measured elevated LV filling pressure may be needed to confirm the diagnosis (for details, see below).

The next step comprises an advanced workup in case of initial evidence of HFpEF/HFmrEF and consists of objective demonstration of structural and/or functional alterations of the heart as the underlying cause for the clinical presentation. Key structural alterations are a left atrial volume index (LAVI) >34 mL/m^2 or a left ventricular mass index (LVMI) ≥115 g/m² for males and ≥95 g/m² for females.[65,67,72] Key functional alterations are an E/e′ ≥13 and a mean e' septal and lateral wall <9 cm/s.[65,67,70,72,80–84] Other (indirect) echocardiographically derived measurements are longitudinal strain or tricuspid regurgitation velocity (TRV).[72,82] An overview of normal and abnormal values for echocardiographic parameters related to diastolic function is presented in *Web Table 4.3*. Not all of the recommended values are identical to those published in previous guidelines, because of the inclusion of new data published in recent reports, in particular by Cabarello *et al.*[70]

A diastolic stress test can be performed with echocardiography, typically using a semi-supine bicycle ergometer exercise protocol with assessment of LV (E/e′) and pulmonary artery pressures (TRV), systolic dysfunction (longitudinal strain), stroke volume and cardiac output changes with exercise.[85,86] Different dynamic exercise protocols are available, with semi-supine bicycle ergometry and echocardiography at rest and submaximal exercise being used most often.[85] Exercise-induced increases in E/e′ beyond diagnostic cut-offs (i.e. >13), but also other indirect measures of systolic and diastolic function, such as longitudinal strain or TRV, are used. Alternatively, invasive haemodynamics at rest with assessment of filling pressures [pulmonary capillary wedge pressure (PCWP) ≥15 mmHg or left ventricular end diastolic pressure (LVEDP) ≥16 mmHg] followed by exercise haemodynamics if below these thresholds, with assessment of changes in filling pressures, pulmonary artery systolic pressure, stroke volume and cardiac output, can be performed.[87]

The diagnosis of HFpEF in patients with AF is difficult. Since AF is associated with higher NP levels, the use of NT-proBNP or BNP for diagnosing HFpEF probably needs to be stratified by the presence of sinus rhythm (with lower cut-offs) vs. AF (higher cut-offs). LAVI is increased by AF, and functional parameters of diastolic dysfunction are less well established in AF, and other cut-off values probably apply. On the other hand, AF might be a sign of the presence of HFpEF, and patients with AF and HFpEF often have

similar patient characteristics. In addition, patients with HFpEF and AF might have more advanced HF compared with patients with HFpEF and sinus rhythm.

Patients with HFpEF are a heterogeneous group with various underlying etiologies and pathophysiological abnormalities. Based on specific suspected causes, additional tests can be performed (*Web Table 4.4*).[71,88–94] However, they can only be recommended if the results might affect management.".

It further states that "Clinicians responsible for managing patients with HF must frequently make treatment decisions without adequate evidence or a consensus of expert opinion. The following is a short list of selected, common issues that deserve to be addressed in future clinical research".

Exploratory experiments in TOPCAT

A larger trial like TOPCAT collected a big amount of markers from the patients enrolled. To exploit this, the first approach we tried was to represent the first three dimensions of the output space, which we remind are the ones that encode the main modes of variation within the population, using several biomarkers. For instance, we represented in shades of gray the estimated glomerular filtration rate (eGFR) as it is a marker of renal function very likely associated to HFpEF. Also, we used body mass index, age, sex and time to event (primary, HF hospitalization and all-cause mortality).

We could only observe differences when representing the eGFR, shown below, where we observe one side of the output space darker than the other side. We remind that in this representation darker means lower, which at translates in impaired renal function. Given the qualitative nature of these results, these were not included in the main section

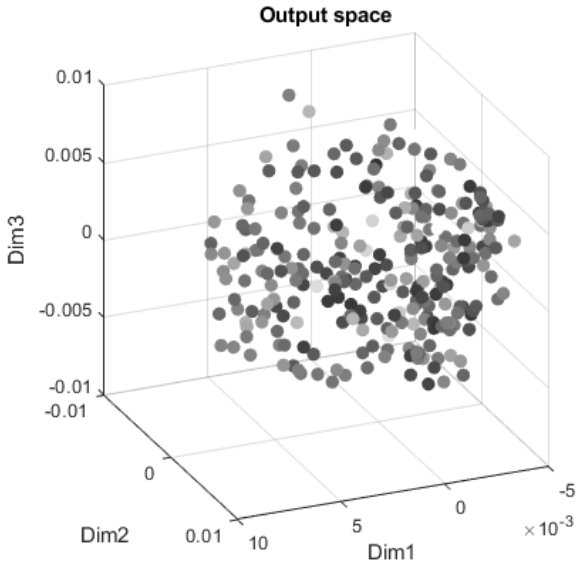

Moreover, we employed the time to event data to run several survival analyses. These were done with a Cox-Regression Proportional Hazards model. In this case, we run the analyses using the first six dimensions as covariates.

We also conducted the same procedure for the solutions of MKL obtained with flows and strains separately and then with a combination of both. In red we showed the models that yielded significant results, meaning that there was a correlation between the position along that dimension and the probability of having an event.

FLOWS AND STRAINS

PRIMARY OUTCOME						
Dimension	1	2	3	4	5	6
b	-0.0064066	-0.1551	0.12577	-0.013152	0.20501	0.07391
Hazard Ratio	0.99361	0.85633	1.134	0.98693	1.2275	1.0767
p-Value	0.96131	0.19857	0.28723	0.90957	0.12604	0.56639
HF Hospitalization						
Dimension	1	2	3	4	5	6
b	-0.36664	-0.25105	0.11349	0.19961	0.43493	0.0032508
Hazard Ratio	0.69306	0.77798	1.1202	1.2209	1.5449	1.0033
p-Value	0.10905	0.10168	0.45281	0.13842	0.022297	0.98426
All Cause Mortality						
Dimension	1	2	3	4	5	6
b	0.19186	0.012653	-0.0056057	-0.018618	0.091715	0.26086
Hazard Ratio	1.2115	1.0127	0.99441	0.98155	1.0961	1.2981
p-Value	0.17531	0.92989	0.9676	0.89886	0.53168	0.08881

FLOWS

PRIMARY OUTCOME						
Dimension	1	2	3	4	5	6
b	0.011409	0.14984	0.28193	0.014479	-0.06909	0.28349
Hazard Ratio	1.0115	1.1616	1.3257	1.0146	0.93324	1.3278
p-Value	0.92415	0.24058	0.020389	0.9042	0.59679	0.007812
HF Hospitalization						
Dimension	1	2	3	4	5	6
b	-0.0036569	0.029014	0.27732	-0.22893	0.15312	0.3511
Hazard Ratio	0.99635	1.0294	1.3196	0.79539	1.1655	1.4206
p-Value	0.98192	0.8466	0.061598	0.13964	0.39141	0.0022468
All Cause Mortality						
Dimension	1	2	3	4	5	6
b	0.008875	0.21365	0.1359	-0.066811	-0.29555	0.05827
Hazard Ratio	1.0089	1.2382	1.1456	0.93537	0.74412	1.06
p-Value	0.94562	0.15081	0.37653	0.61878	0.037386	0.67214

STRAINS

PRIMARY OUTCOME						
Dimension	1	2	3	4	5	6
b	0.083638	0.33246	0.2259	0.0071157	0.26027	0.0561
Hazard Ratio	1.0872	1.3944	1.2534	1.0071	1.2973	1.0577
p-Value	0.42663	0.0006683	0.020774	0.93559	0.005719	0.57393
HF Hospitalization						
Dimension	1	2	3	4	5	6
b	-0.091077	0.39807	0.21339	0.10423	0.27887	-0.06062
Hazard Ratio	0.91295	1.489	1.2379	1.1099	1.3216	0.94118
p-Value	0.51303	0.0010527	0.074642	0.31809	0.011662	0.62849
All Cause Mortality						
Dimension	1	2	3	4	5	6
b	0.16499	0.18297	0.091836	0.011885	0.23205	0.23518
Hazard Ratio	1.1794	1.2008	1.0962	1.012	1.2612	1.2651
p-Value	0.1774	0.12096	0.43007	0.91339	0.042266	0.047776

We shall firstly address that these results are not straight-forward to analyze, they are rather an interesting insight into the possibilities of the analysis of the output space. Even though, we obtained some dimensions associated with a significant p-value, thus understanding the information encoded in those dimensions may prove of utility at the time of clinical interpretation.

Next on, we computed the difference between the solutions obtained with the different combinations of features. We did so by computing the kernel function of each solution and seeing the correlation between the different kernels.

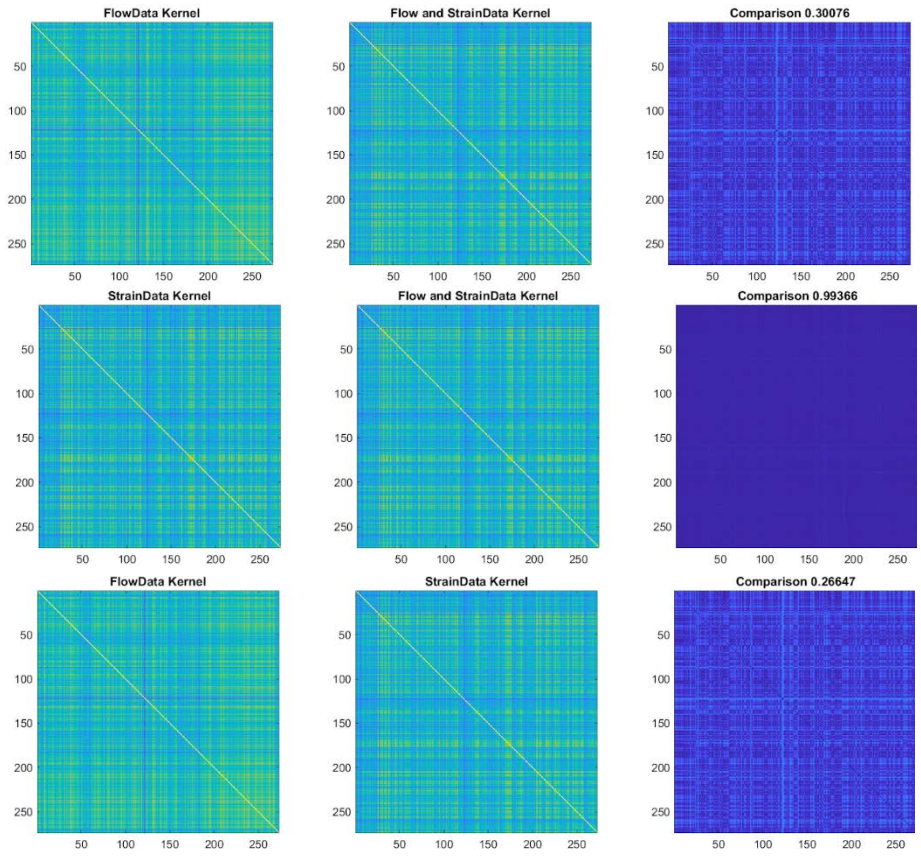

In this experiment we observed a very strong correlation between the solution obtained with the strain feature and the one which combines both flow and strain. This is not trivial to explain, but a cause may lie in the similarity in the strain patterns among all patients, whereas flow patterns are more diverse. As explained in the paper by Sanchez-Martinez et al. (Characterization of myocardial motion patterns by unsupervised multiple kernel learning. Medical image analysis. 2017), MKL gives more weight to correlated features rather than those that differ more between patients.

Echocardiographic Image Analysis Platform Tutorial

A video tutorial of the platform can be found here:
https://www.youtube.com/watch?v=tWI-FZ0aZYY

We will now proceed to explain step by step how the platform works, showing all of its capabilities.

Once the platform is launched, the user will face the following interface.

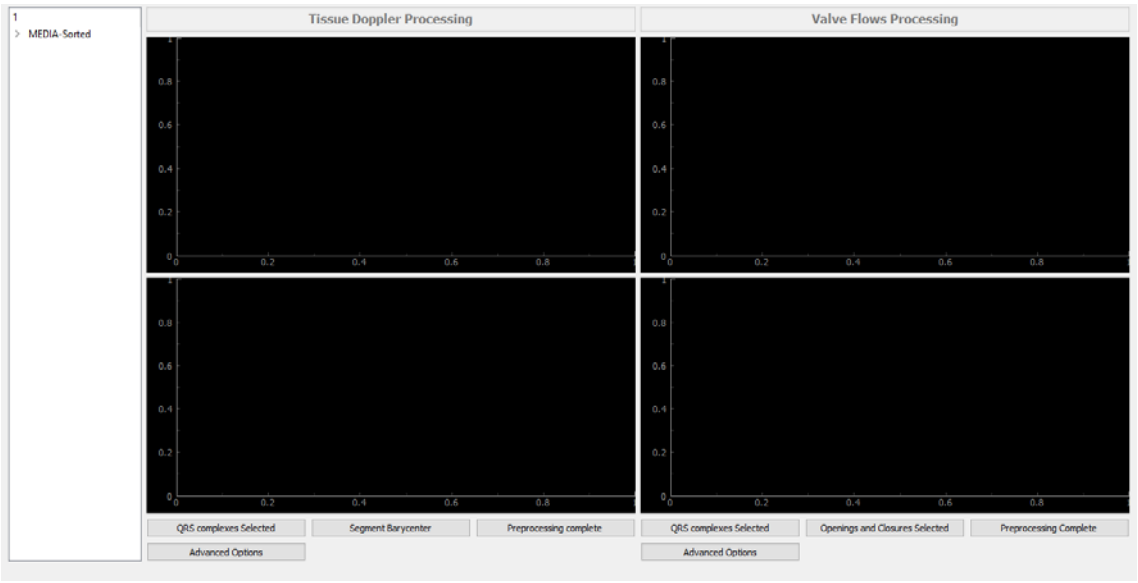

Next, the user will have to select the specific patient he wants to process in the left column, where a tree will represent the database, containing all the patients.

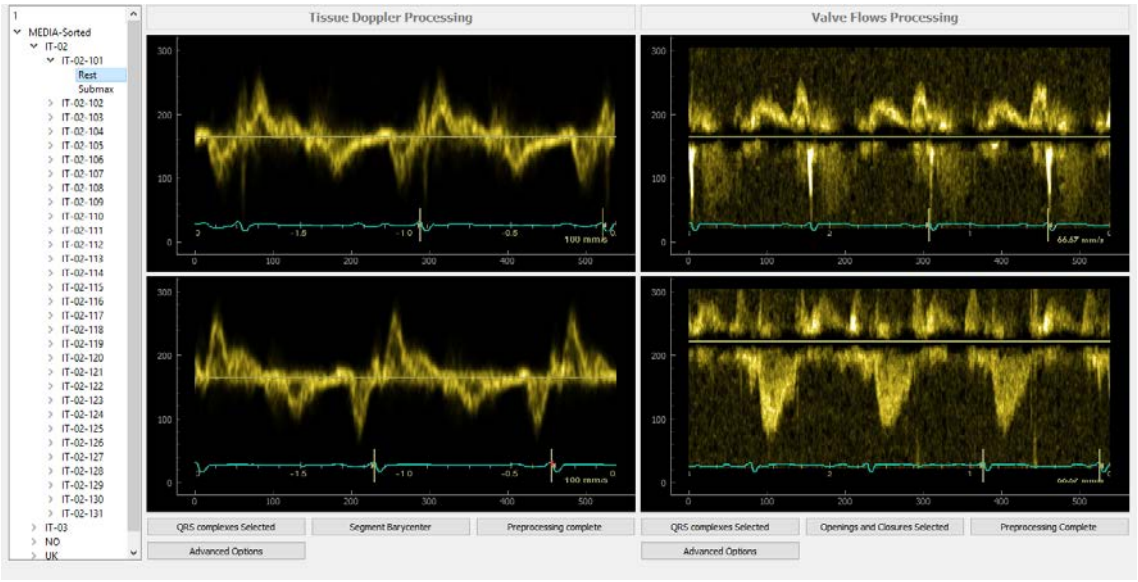

When the case is clicked, the images corresponding to that patient will be loaded as shown in the image. On the left side will be the tissue Doppler images and on the right will be the blood flow velocities.

Starting with the processing of the TDI images, the user can start by clicking the ECG onsets, which will appear as a vertical white line.

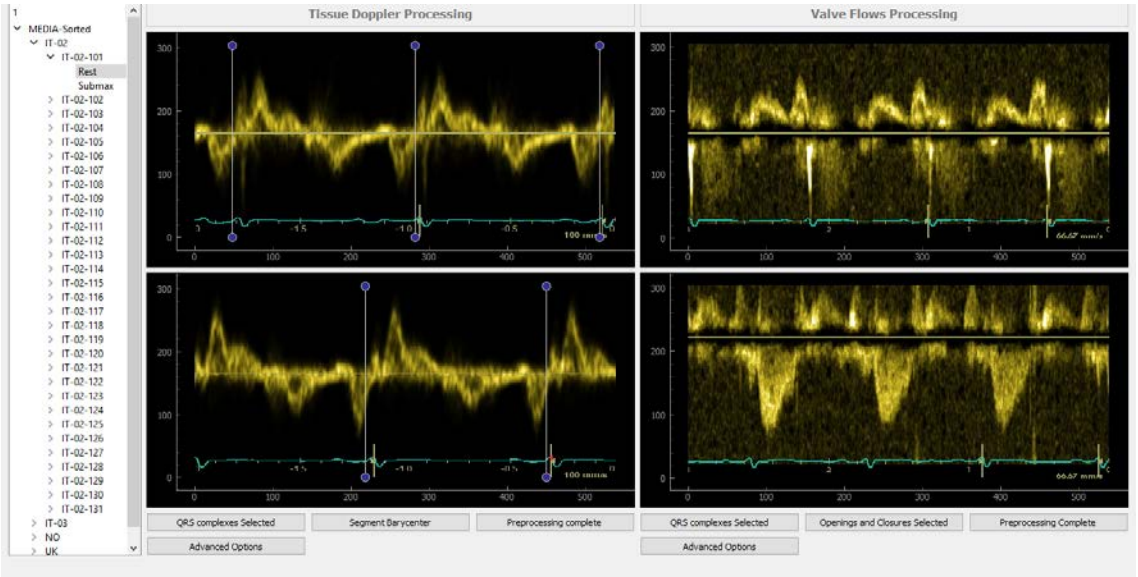

When all ECG onsets have been determined, the button QRS Complexes Selected needs to be clicked, it will store the timings for the ECG onsets and represent them with a red dashed line as in the next image.

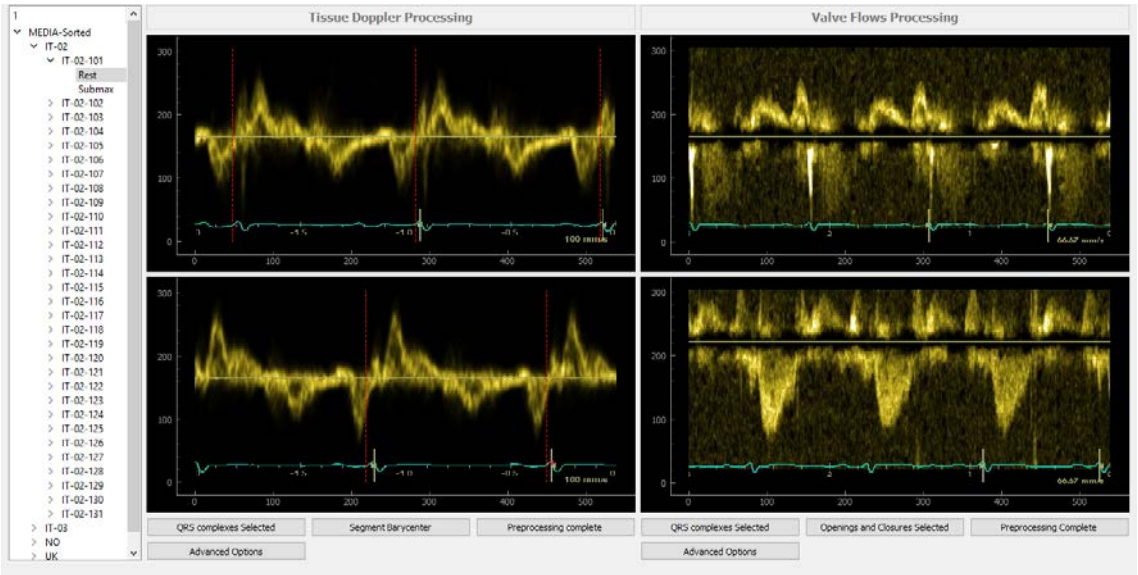

Following, the button Segment Barycenter needs to be clicked. It will run the image processing algorithms needed to obtain the profile, which will be shown on top of the image in blue. This is represented in the next caption.

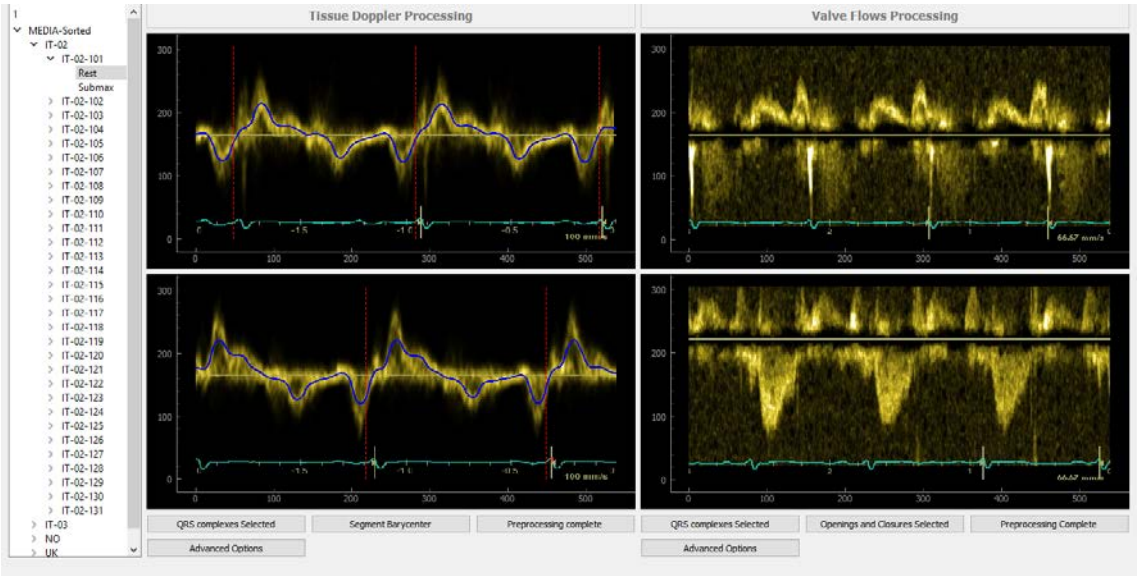

If the result of the segmentation is not good enough, the Advanced Options button can be pressed. It will open a new window, where two parameters can be modified for improving the segmentation. The result of changing the parameters will be shown in real time.

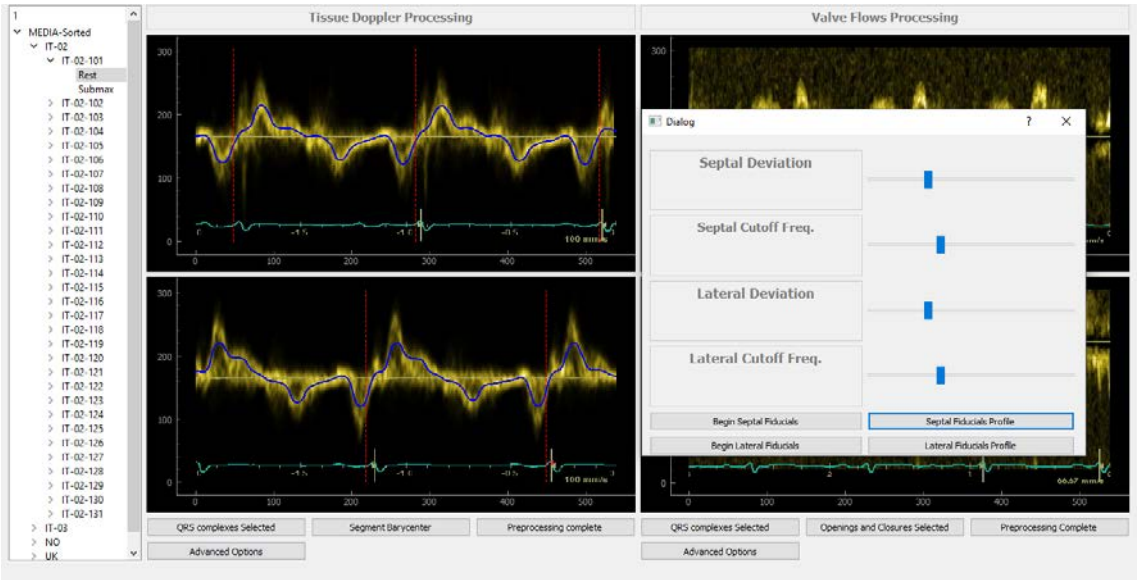

If the result after changing the parameters is good, the user can proceed to close the window and click on the Preprocessing complete button. When this is done, the averaged descriptor will be plotted and stored.

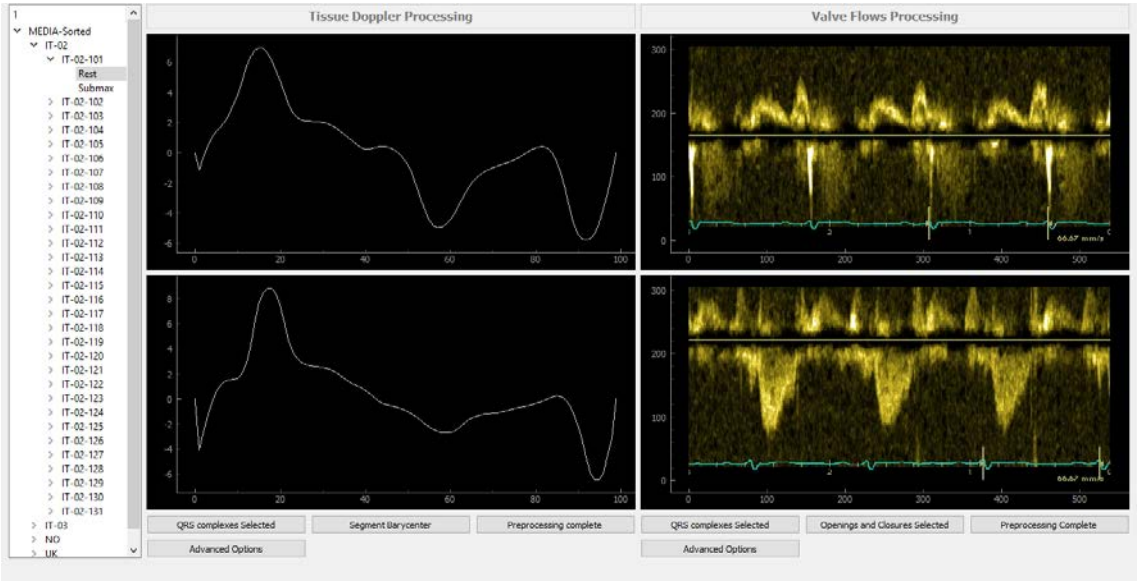

For the sake of showing the possibilities of the platform, we will now proceed to manually segment the image using fiducial points. This is to be done when the image is so noisy that automatic tools do not perform well enough. The first thing that needs to be done is to open the advanced options window by clicking on its button.

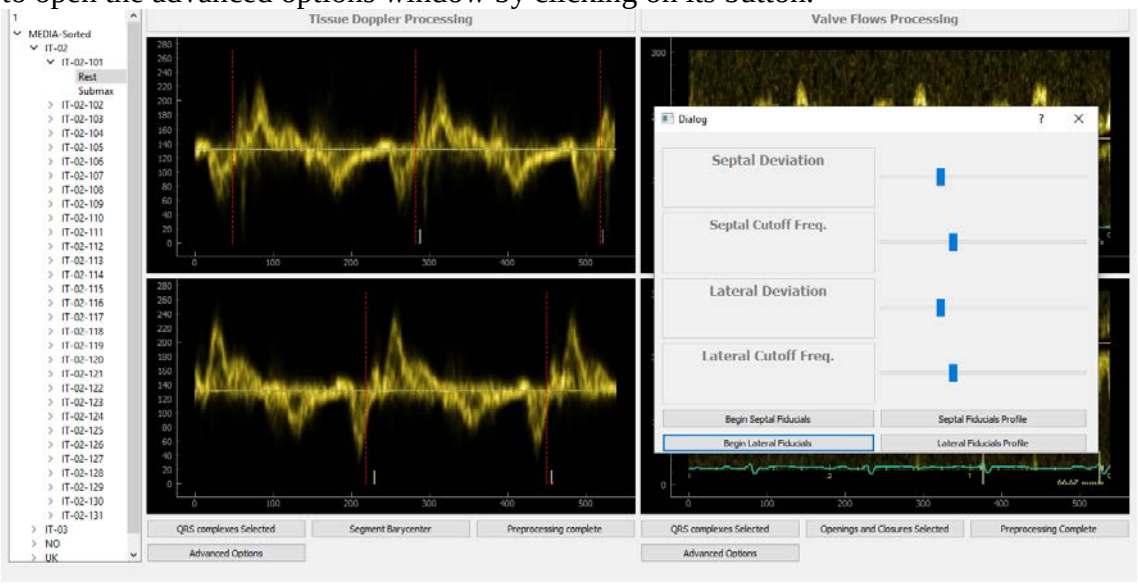

Then the buttons Begin septal/lateral fiducials should be clicked. Once this is done the user can proceed to place point on top of the signal by double clicking. The spline connecting the points will appear as soon as there are more than three points and it will show the result in real time as mor points are added.

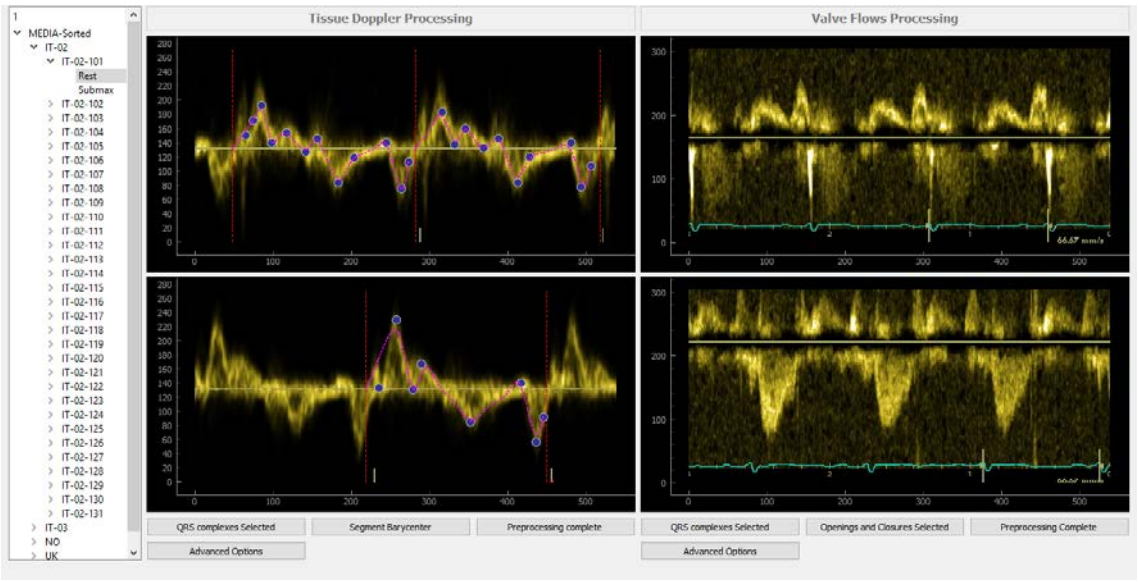

When the user has finished placing fiducial points, the advanced options window needs to be opened to press the septal/lateral fiducials profile button. This will average the cycles, plot the result and store it.

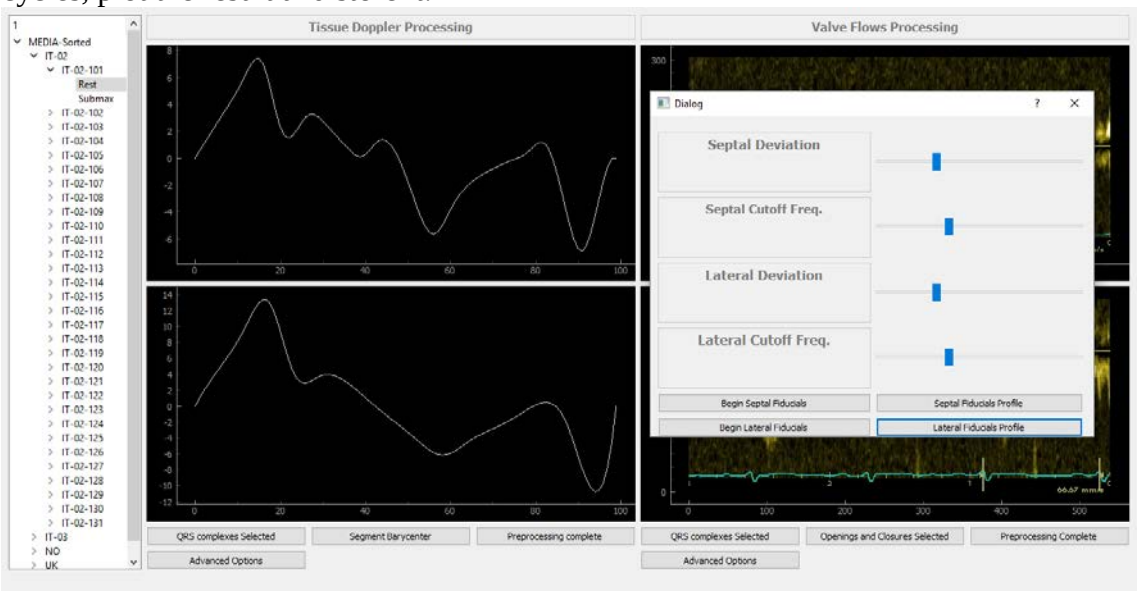

Now on to the flow velocity segmentation. As in TDI, the user starts by selecting the ECG onsets and clicking the QRS complexes selected button.

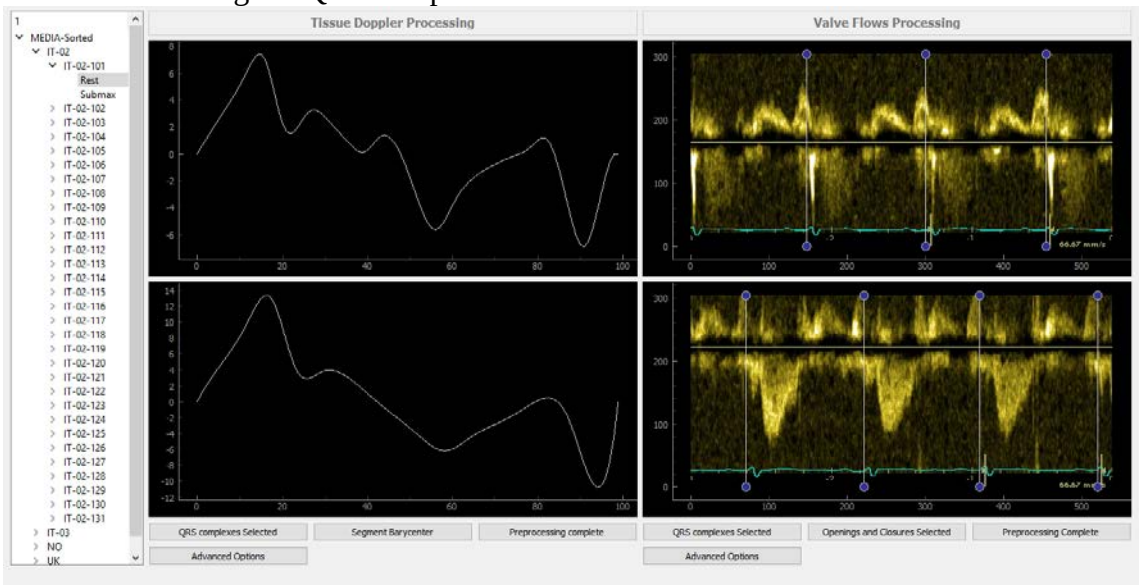

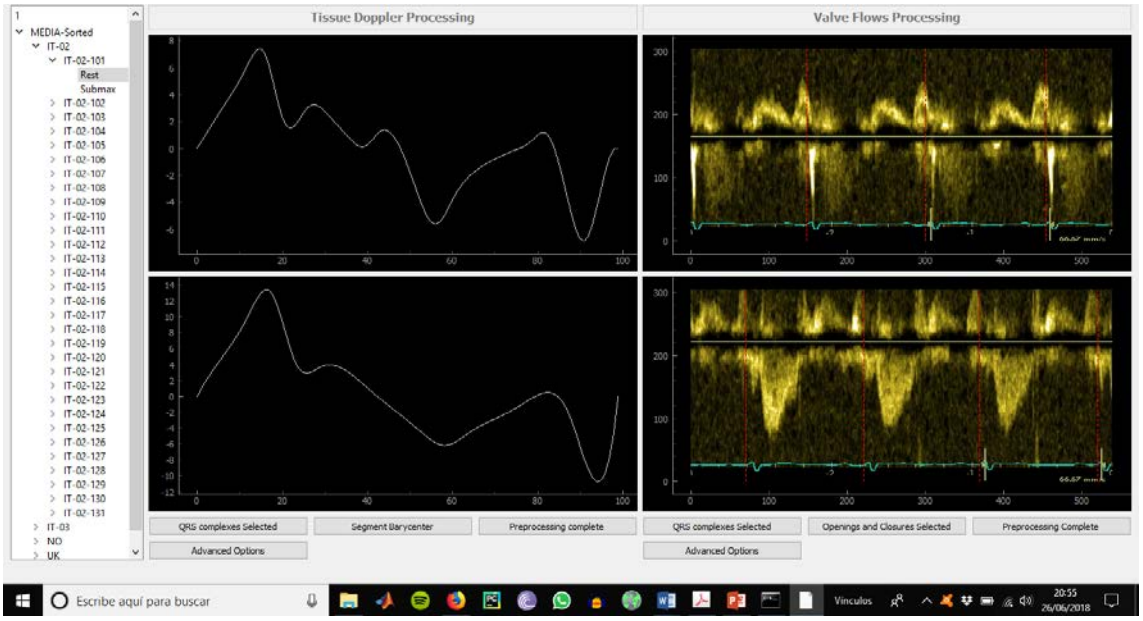

The onsets will appear as red dashed lines and the user can proceed to select the opening and closures of the valves. Which will appear in cyan. This is needed as one of the features of the platform still in development is to store the times between the ECG onsets and the openings and closures of the valves, which can be used as machine learning descriptors.

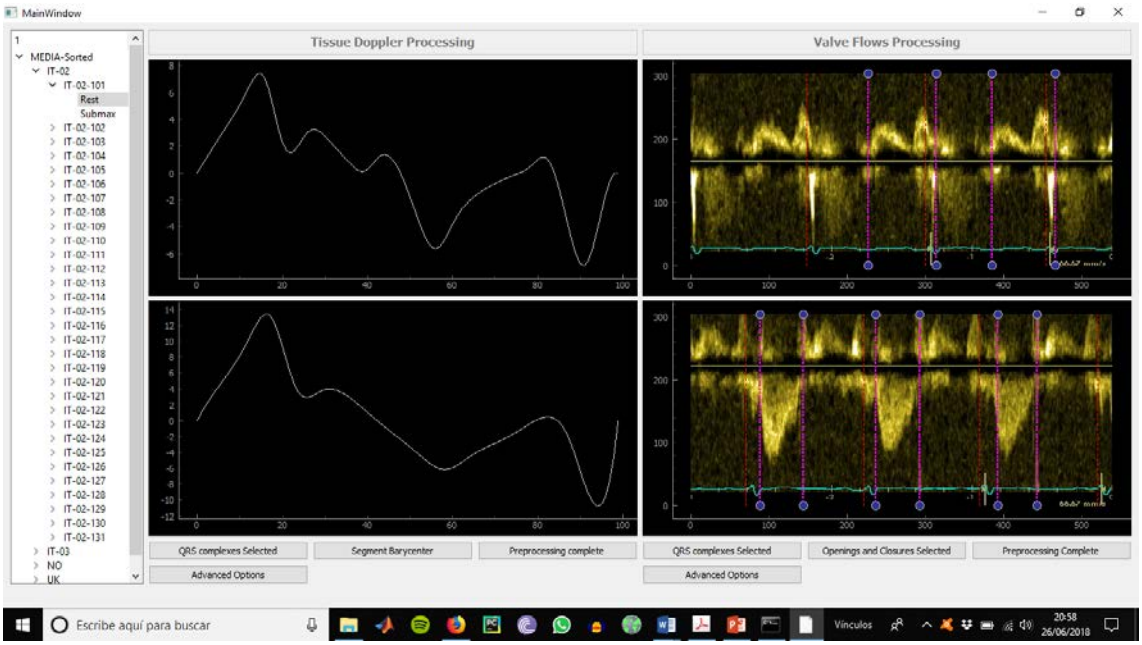

When this is done, the user shall click on the Openings and Closures Selected button. This will run the segmentation algorithms and plot the contour of the segmentation on top of the image.

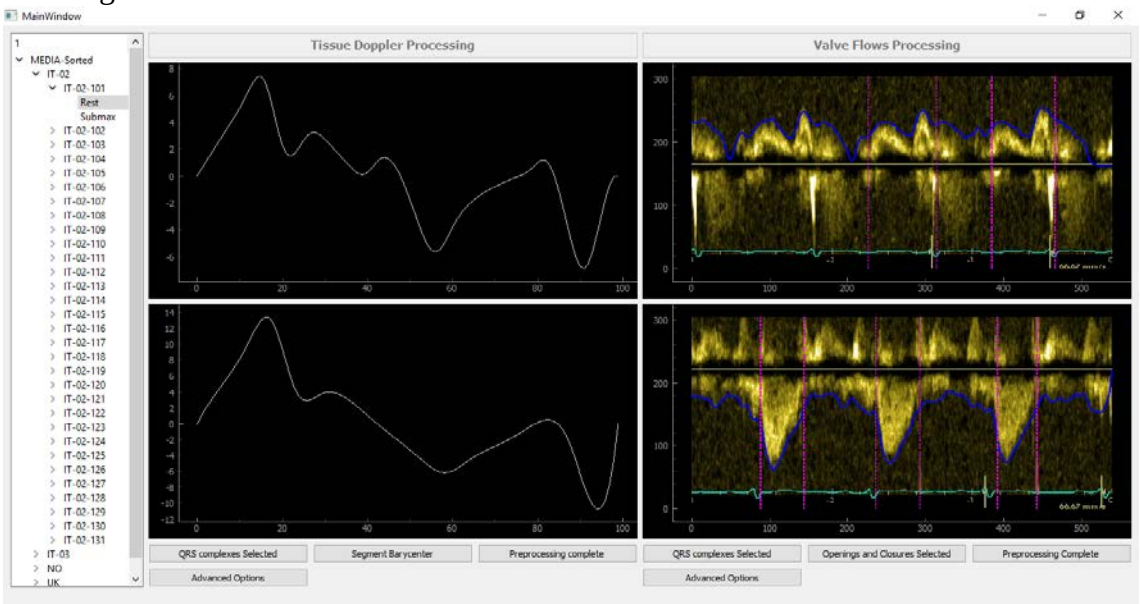

If needed, the user can open the advanced options window by clicking on its button and tune the segmentation parameters to refine the segmentation. This is illustrated below.

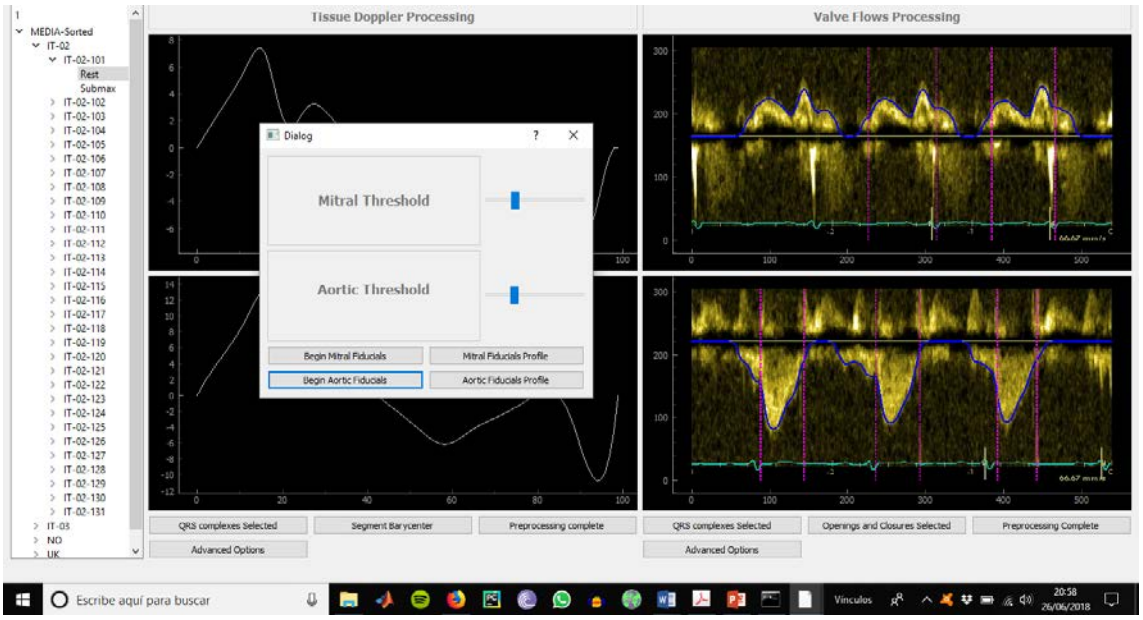

Once the segmentation is good enough, the user can close the window and click the Preprocessing complete button. This will plot the final descriptors which will be stored.

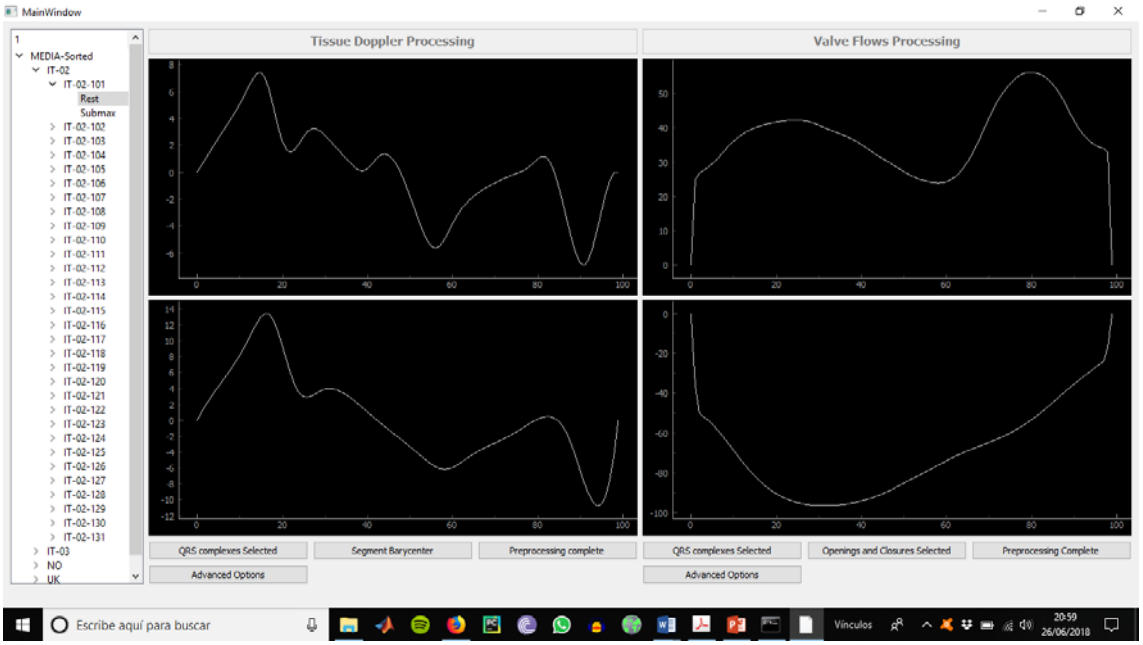

We also represented the placing of fiducial points for valve flow, although the procedure is the same as in the TDI images.